

MEASURING SURFACE SHAPE OF TRANSPARENT
OBJECTS BASED ON THE ANALYSIS OF
POLARIZATION, THERMAL RADIATION AND
GEOMETRICAL PROPERTY
偏光・熱放射・幾何学的性質の解析に基づく透明物体の表面
形状計測

by

Daisuke Miyazaki
宮崎 大輔

A Master Thesis
修士論文

Submitted to
the Graduate School of
the University of Tokyo
on February 5, 2002
in Partial Fulfillment of the Requirements
for the Degree of Master of Science
in Information Science

Thesis Supervisor: Katsushi Ikeuchi 池内 克史
Professor of Information Science

ABSTRACT

In the field of computer vision, many methods which measure the surface shape of opaque objects have been proposed; however, a successful method which measures the surface shape of transparent objects such as glasses has never been developed. In this paper, we propose a convenient and beneficial method to measure the surface shape of transparent objects.

The light which is reflected from the surface of the object is partially polarized. The degree of polarization depends upon the incident angle which, in turn, depends upon the surface normal of the object; thus, we can obtain the surface normal of the object by observing the degree of polarization. But unfortunately, the correspondence between the degree of polarization and the surface normal is not 1 to 1; thus, to obtain the correct surface normal, we had to solve this ambiguity problem. To disambiguate this problem, we took two approaches. One was to use the phenomenon of thermal radiation; the other was to use the differential-geometrical characteristics of the object surface.

The light emitted from the object caused by heating up the object is called thermal radiation. Because thermal radiation is also a light, it partially polarizes when emitted from the object. We heated up the object, and we succeeded in solving the ambiguity problem by observing the degree of polarization of the radiated infrared light.

We also developed a method for using the differential-geometrical property of the object surface. This method solves the ambiguity by comparing two types of data, one of which is obtained straightforwardly observing the object, while the other is obtained by observing the object while it is inclined at a slight angle. In this method, we have to compare these two data at identical points on the object surface. We find two identical points by considering the invariant value on the object surface, and we compare the data of polarization at these two points. We discuss the relationship between the geometrical property on object surface and the degree of polarization based on the knowledge of differential geometry, and we propose a method for matching two pieces of polarization data at identical points on the object surface.

In this paper, we describe how we applied both the method using thermal radiation and the method using geometrical property to real transparent objects in order to obtain the correct surface normal of transparent objects.

論文要旨

コンピュータビジョンの分野では不透明な物体の表面形状を計測する手法は多々提案されているにも関わらず、ガラスなどの透明な物体の表面形状を計測する有力な手法は未だ確立されずにいる。本論文では、透明物体の表面形状を計測する、簡便で有用な手法を提案する。

物体表面を反射した光は部分偏光する事が知られており、その偏光の度合いは入射角に依存する。入射角は物体の表面法線に依存するので、偏光の度合いを観測する事により、物体の表面法線を求める事が可能である。しかし、残念ながら偏光度と表面法線は1対1には対応しておらず、正しい表面法線を得るためにこの表面法線の曖昧性の問題を解決する必要がある。そこで、異なる2つのアプローチからこの曖昧性を除去する事にした。1つは熱放射現象を利用したもので、もう1つは物体表面の微分幾何学的性質を利用したものである。

物体に熱を加えた事により物体から発する光を熱放射光という。熱放射光であっても光である以上、光が物体表面から出てくる時に部分偏光する。我々は、物体を熱し、物体から放射された赤外光の偏光度を観測する事によって、上記の曖昧性の問題を解決する事に成功した。

さらに我々は、物体表面の微分幾何学的性質を利用した手法も開発した。この手法とは、物体をそのまま観測したデータと、物体をわずかに傾けて観測する事により得られたデータを比較する事によりこの曖昧性を除去するという手法である。この際、得られた2つのデータを、物体表面上の同一な点で比較する必要がある。物体表面上の不変量を用いて物体表面上の同一な点を探し、その2点で偏光データの比較を行うのである。我々は、微分幾何学の知識を用いて、物体表面の幾何学的性質と偏光度の関係を論じ、2つの偏光データにおける物体表面上の同一な点を探し出す手法を提案した。

最後に、熱放射を利用した手法と物体表面の幾何学的性質を利用した手法それぞれを実際の透明物体に対して適用し、透明物体の表面法線を正しく得る事ができる事を示した。

Acknowledgements

Thanks for Katsushi Ikeuchi for useful advises, guidances, and discussions. I appreciate all the members in Ikeuchi laboratory for providing me a pleasant environment to keep on studying well. Especially I thank Megumi Saito's effort, because this paper have never been accomplished without her previous work.

Contents

1	Introduction	4
2	Polarization Analysis	7
2.1	Fresnel Reflection	7
2.2	Polarization Degree	8
3	Thermal Radiation	12
3.1	Introduction	12
3.2	Kirchhoff's Law	14
3.3	Emitted Light	14
3.4	Polarization Degree of Thermal Radiation	15
4	Object Rotation	18
4.1	Introduction	18
4.2	Gaussian Curvature	19
4.3	Surface Classes	20
4.4	Folding Point	22
4.5	Brewster Segmentation	27
4.6	Matching Point	30
4.7	Folding Point of Polarization Degree	33
4.8	Difference of Polarization Degree	35
5	Experiments	37
5.1	Experimental Setup	37
5.1.1	Experimental Setup of Visible Light	37
5.1.2	Experimental Setup of Infrared Light	37
5.2	Measurement	38
5.2.1	Measurement of Non-rotated Object in Visible Light Domain	38

5.2.2	Measurement of Thermal Radiation	39
5.2.3	Measurement of Rotated Object	39
5.3	Experimental Result	40
5.3.1	Experimental Result of Thermal Radiation Method	40
5.3.2	Simulational Result of Object Rotation Method	41
5.3.3	Experimental Results of Object Rotation Method	42
6	Conclusions	48
A	Theory of Optics (In More Detail)	54
A.1	Maxwell's equations	54
A.2	Electric Field and Magnetic Field	56
A.3	Poynting Vector and Intensity	58
A.4	Fresnel formulae	59
A.5	Derivation of Intensity Ratio	62
A.6	Graph of Intensity Ratio	63
B	Gaussian Mapping	65
C	Fitting Sine Curve	68
D	Relaxation Method	70
E	English-Japanese Dictionary for Technical Terms	71
F	References Written in Japanese	74
F.1	References for Computer Visions	74
F.2	References for Optics	74
F.3	References for Thermodynamics	75
F.4	References for Differential Geometries	76

List of Figures

2.1	Fresnel reflection	8
2.2	Surface normal of the object	9
2.3	Relation between the degree of polarization and the incident angle ($n = 1.5$)	11
3.1	Energy distribution of blackbody	13
3.2	Polarization degree of (a)thermal radiation (infrared light) ($n = 1.5$), and (b)reflected light (visible light) ($n = 1.5$)	16
4.1	Normal section	20
4.2	Surfaces classified by Gaussian curvature	21
4.3	Curves classified by curvature	24
4.4	Gaussian mapping of some patches	26
4.5	Coordinates of surface normal	28
4.6	Object rotation	30
4.7	Gaussian mapping of B-B region	31
4.8	Matching Point	32
4.9	Graph of derivative of polarization degree.	35
5.1	Experimental setup	38
5.2	Error characteristics of the spherical object	40
5.3	The resulting shape of the shellfish-shaped object	41
5.4	Simulation result of the object No.1	42
5.5	Simulation result of the object No.2	43
5.6	Simulation result of the object No.3	43
5.7	The result of the real hemisphere object	44
5.8	The graph of the polarization degree of the hemisphere object	45
5.9	The result for the bell-shaped real object	47

5.10 The result of the real bell-shaped object	47
A.1 Electric vector	59
A.2 Magnetic vector	60
A.3 Amplitude reflectivity and amplitude transmissivity	62
A.4 Graphs of intensity ratios	64
B.1 Gaussian mapping	66
B.2 Three examples of Gaussian mapping	67

List of Tables

4.1	Surface classes and curvatures	23
5.1	Error of plastic transparent hemisphere	45

Chapter 1

Introduction

Recently, techniques for modeling objects through observation have been extensively investigated. Such modeling has a wide area of applications, including virtual reality and object recognition. Geometry, one of the most important aspects of modeling, can be used to create a model based on measuring the shape of an object.

Many techniques to measure object shape have been developed in the field of optical engineering. These techniques can be classified into two categories: point and surface types. A point type method, such as a laser range sensor, measures object shape by projecting a spotlight, often a laser beam, over the object surface, and by measuring the returned timing of the returned direction. A surface method, such as Moire topography, determines the shape of an object by projecting a planar light and measuring the interference of the light with the surface.

The computer vision community has extensively developed additional techniques. Shape-from-shading, for example, analyzes shading information in an image with a reflectance map in order to relate image brightness to surface orientations. Photometric stereo obtains information from three images, taken from the same position, under three different illumination conditions. Binocular stereo and motion analysis use image differences in a series of images taken from different positions.

Most of these methods are, however, designed to obtain the shape of opaque surfaces. Namely, these techniques are based on analysis of the body reflection component of an object surface. Models of transparent objects, which have only surface reflection, cannot be created using these techniques. Few extant methods attempt to determine object shapes through surface reflection.

With regard to surface reflection, Ikeuchi [1] proposed to determine the reflectance of a metal surface using photometric stereo. When exposed to three extended light

sources, a metal surface generates different illumination distributions over the surface. The application of the photometric stereo method to these illumination distributions allows the shape of a metal surface to be determined. Nayar et. al. [2] extended the method by using continuous illumination distribution, referred to as a photometric sampler. Their method determines not only surface shape but also surface reflectance parameters. Sato et. al. [3] analyzed color images in a similar setting, and determined the shape and reflectance of shiny objects for computer graphics purposes, and Oren and Nayar [4] proposed a method using surface reflections and motion to determine surface shape.

Surface reflection can also be analyzed through the degree of polarization, as demonstrated by Kosikawa [5], who proposed to use the degree of polarization, employing polarized light sources to determine the shape of metal surfaces. Later, Koshikawa and Shirai [6] applied this method to the recognition of objects. Wolff [7] proposed to analyze the degree of polarization in visible light for that same purpose. Wolff et. al. [8] indicated that the surface normal of the object surface is constrained by analyzing the polarization of the object; Rahmann [9] proposed the method of recovering the shape of specular surfaces from polarization. Jordan et. al. [10, 11] and Wolff et. al. [12] analyzed the degree of polarization in the infrared wavelength.

A transparent surface also has surface reflection components. Szeliski et. al. [13] analyzed the movement of surface reflection components on a transparent object, and separated surface reflection from background images. Schechner et. al. [14] proposed a method with which to determine only the surface reflection component, using the degree of polarization. That method also addressed the extraction of information about the orientation of transparent planes. For graphics applications, Zongker et. al. [15] and Chuang et. al. [16] developed a method with which to generate the appearance of a transparent object from a series of images taken under different background conditions. These methods, however, do not totally provide the shape information of transparent objects of arbitrary shape.

Saito et. al. [17, 18] employed the analysis of the degree of polarization and developed a method with which to measure the surface of a transparent object. Employing an extended light source originally developed by Nayar et. al. [2], they illuminated a transparent object and were able to obtain surface reflection components over the entire visible surface. Then, by measuring the degree of polarization, they determined surface orientations. Unfortunately, however, the degree provides two solutions corresponding to one polarization degree. Thus, the method can be applied to measuring a limited class of objects or to surface inspection where rough surface orientation is

predetermined; it cannot be applied to a general class of objects.

In this paper, we propose to disambiguate these two solutions by two novel methods. One is to introduce the polarization degree in the infrared wavelength, and the other is to introduce the polarization analysis by rotating the object.

The first method, using infrared wavelength, obtains the degree of polarization in the visible wavelength, which was likewise obtained in our earlier method. One polarization degree measured corresponds to two surface orientations. The polarization degree in the infrared wavelength provides a single surface orientation to one polarization degree. Thus, by simultaneously measuring the degree in the infrared domain, we can uniquely determine the surface orientation. The measurement in the infrared wavelength cannot be used directly because the polarization degree is relatively low in some areas, and it is therefore better to use this measurement solely for judgment purposes.

The second method, using object rotation, obtains two data of polarization from two different views, as is done in the binocular stereo method. Actually, we did not set two cameras; for the purpose of experimental setup convenience, we fixed the camera and tilted the object only slightly to obtain two data of two different views. This new method first obtains the degree of polarization, which was likewise obtained in our earlier method. One polarization degree measured corresponds to two surface orientations. The polarization degree of a novel view disambiguates this problem. By comparing the polarization degree at the same surface point of each polarization data, we determine the unique surface orientation.

In Chapter 2, we present the background theory of polarization and then develop an underlying algorithm to determine surface orientation up to two possible incident angles, using the polarization. In Chapter 3, we describe a method with which to obtain surface shape using the polarization degrees in both visible and infrared wavelengths. In Chapter 4, we describe the method for disambiguating the possibility in the incident angle by rotating the object. In Chapter 5, we describe the apparatus of these two methods and the experimental results. Chapter 6 concludes the paper.

Chapter 2

Polarization Analysis

2.1 Fresnel Reflection

The light that reflects from the surface of most types of objects can be separated into two major components, surface reflection and body reflection. Incident light partly reflects at the surface and partly penetrates inside the object. The light that penetrates inside an opaque object randomly reflects some of the pigments inside the object and is emitted into the air. The light that specularly reflects at the surface is called the surface reflection, and the light that is diffusely emitted into the air from inside the object is called the body reflection [19]. We focus only on transparent objects in this paper, analyzing surface reflection rather than body reflection.

In this section, we present a brief overview of the basic equation of reflection and refraction [20]. In Figure 2.1, let us consider the case in which a light hits the interface surface between two materials, the refractive indices of which are denoted as n_1 and n_2 , respectively. Here we assume that the interface surface lies on the X-Y plane without loss of generality. One part of the light is reflected from the interface surface, while another part penetrates the surface and is refracted when it enters the second material. Because we assume that both materials are transparent, we can ignore the component to be absorbed. We denote the incident light, the reflected light, and the transmitted light as the subscripts a , r , and t , respectively, and identify the parallel and perpendicular components to the X-Z plane as p and s , respectively. The incident, reflecting, and transmitting angles are defined as θ_1 , θ'_1 , and θ_2 , respectively, as shown in Figure 2.1. Given that the incident and the reflected light pass through the same materials, $\theta_1 = \theta'_1$, we can define the parallel and perpendicular reflectance ratios, F_p

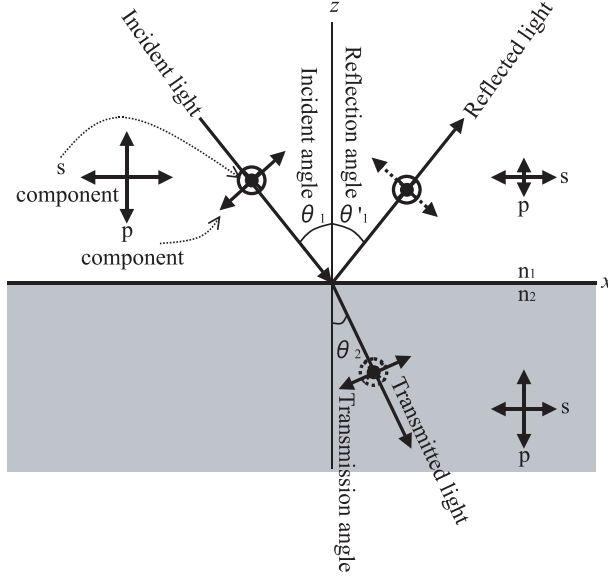


Figure 2.1: Fresnel reflection

and F_s , respectively, as

$$\begin{aligned}
 F_p &= \frac{I_{rp}}{I_{ap}} = \frac{\tan^2(\theta_1 - \theta_2)}{\tan^2(\theta_1 + \theta_2)} \\
 F_s &= \frac{I_{rs}}{I_{as}} = \frac{\sin^2(\theta_1 - \theta_2)}{\sin^2(\theta_1 + \theta_2)}
 \end{aligned}
 \tag{2.1}$$

where I_{ap} is the component parallel to the X-Z plane of the incident light, and I_{rp} is that of the reflected light. I_{as} is the component perpendicular to the X-Z plane of the incident light, and I_{rs} is that of the reflected light. From the above equation, an incident angle to make $F_p = 0$ can be obtained. This incident angle is referred to as the Brewster angle, θ_B . The Brewster angle is obtained by substituting $\theta_1 + \theta_2 = \pi/2$ (namely, $F_p = 0$) into Snell's equation, $n_1 \sin \theta_1 = n_2 \sin \theta_2$, as

$$\tan \theta_B = \frac{n_2}{n_1}.
 \tag{2.2}$$

2.2 Polarization Degree

An interface surface of a transparent object causes little diffuse reflection or absorption; under the condition of the reflected light, the incident and reflecting angles are the

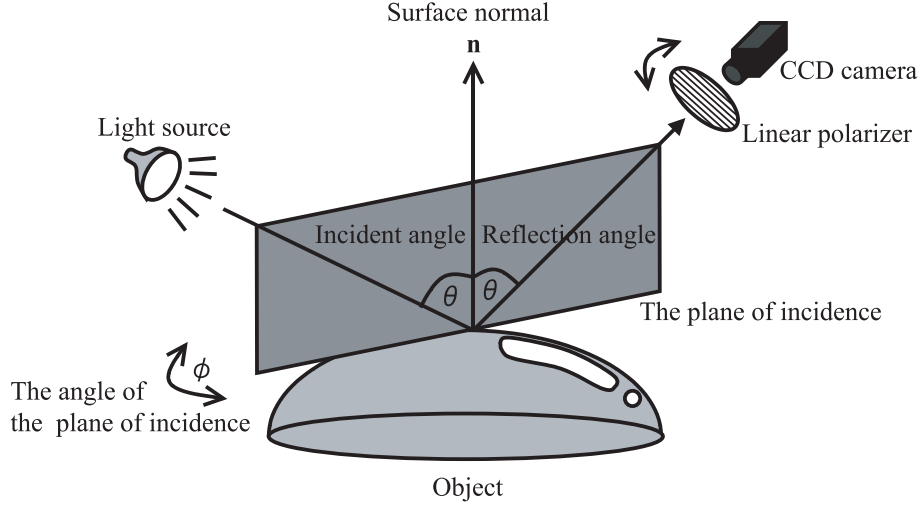


Figure 2.2: Surface normal of the object

same. Thus, once the reflecting angle and the orientation of the plane of incidence are known, we can determine the surface orientation with respect to the viewer, as shown in Figure 2.2. Here the plane of incidence is the one on which the light source, the surface normal, and the viewer vectors lie. We will denote the direction of the plane of incidence and the reflecting angle as ϕ and θ , respectively. We will determine these two angles by using the degree of polarization of reflected light.

Generally speaking, natural light is unpolarized; it oscillates in all directions on the plane of oscillation, which is perpendicular to the path of the light. Natural light, however, becomes polarized once it goes through a polarization material or is reflected from a surface. We will measure the degree of polarization for this purpose.

As shown in Equation (2.1), the intensity varies depending upon the direction on the plane of oscillation and therefore, a difference can be observed when the polarization filter is rotated in front of a CCD camera. The variance is described as a sinusoidal function of rotation angles. We will denote the maximum and minimum brightness in the observed intensities as I_{\max} and I_{\min} . Given that the sum of the maximum and minimum brightness is the total brightness of the reflected light, I_{specular} ,

$$I_{\max} = \frac{F_s}{F_p + F_s} I_{\text{specular}}, \quad I_{\min} = \frac{F_p}{F_p + F_s} I_{\text{specular}}. \quad (2.3)$$

By this equation, the direction parallel to the plane of incidence provides the minimum brightness I_{\min} . Namely, by measuring the angle to give the minimum

brightness, we can determine the direction of the plane of incidence, ϕ . There are two possible directions of the plane of incidence, ϕ_1 and ϕ_2 , which are definable as $\phi_2 = \phi_1 + \pi$. We assume the object as a closed smooth object and has no dimples (=concavity in a convexity), thus, we can determine the surface normal at the occluding boundary; the surface normal heads toward the outside of the object at the occluding boundary, thus, we can choose the correct direction of the plane of incidence, ϕ , at the occluding boundary. The surface normals on any neighboring points on the surface have similar value due to the smoothness of the surface. We can determine the correct direction of the plane of incidence, ϕ , of a certain surface point if the ϕ of the neighboring points are already determined. By using the ϕ at the occluding boundary as an initial condition, we propagate the constraint of ϕ throughout the surface, and finally we determine the whole ϕ over the surface. We disambiguate the ambiguity of ϕ by this method.

The definition of the degree of polarization (*or* polarization degree) is,

$$\rho = \frac{I_{\max} - I_{\min}}{I_{\max} + I_{\min}}. \quad (2.4)$$

The degree of polarization is 0 when the light is unpolarized, whereas it is 1 when the light is linearly polarized. The linearly polarized light is observed when the parallel component becomes 0. This occurs when the incident angle and the reflecting angle are at the Brewster angle.

By substituting Equation (2.3) and (2.1) into Equation (2.4) with Snell's law, we can represent the degree of polarization, ρ , as

$$\rho = \frac{2 \sin^2 \theta \cos \theta \sqrt{n^2 - \sin^2 \theta}}{n^2 - \sin^2 \theta - n^2 \sin^2 \theta + 2 \sin^4 \theta}. \quad (2.5)$$

The degree of polarization is a function of the refractive index, n ($= n_2/n_1$), and the incident angle, θ . Thus, by obtaining the degree of polarization from the data, we can determine the incident angle, θ , given the refractive index n .

Figure 2.3 shows the relation between the degree of polarization and the incident angle. Here, the horizontal and vertical axes denote the incident angle and the degree of polarization, respectively. We can obtain the incident angle from the observed degree of polarization even if we do not know the intensity of the light source. The function has an extreme at the Brewster angle. From this function, an observed degree of polarization provides two possible incident angles, except at the Brewster angle. It is necessary to have a method to resolve this ambiguity. In this paper, we propose to solve this problem by two methods, one by considering the polarization of far infrared light, and the other by comparing two polarization data through rotating the object.

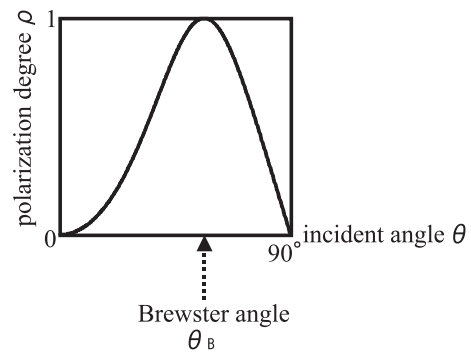


Figure 2.3: Relation between the degree of polarization and the incident angle ($n = 1.5$)

Chapter 3

Thermal Radiation

In this chapter, we explain the method to solve the ambiguity by introducing thermal radiation.

3.1 Introduction

Heat energy can propagate through space. This phenomenon is referred to as heat propagation. A blackbody can completely absorb the heat energy radiated. According to Kirchhoff's law, the ratio between radiant and incoming heat energy is independent of the object; rather, it is dependent only on the temperature of the object. A blackbody, which completely absorbs energy, can also radiate more energy than any other objects that have the same temperature.

From the Stephan-Boltzman law, radiation energy, W , from the blackbody at the temperature T is

$$W = \sigma T^4 \tag{3.1}$$

where σ is the Stephan-Boltzmann coefficient and $\sigma = 5.67 \times 10^{-8} \text{ [W/m}^2\cdot\text{K}^4]$. Given that any object has a positive temperature, any object should radiate energy.

A blackbody has an energy distribution, as shown in Figure 3.1. From the figure, it is apparent that the extremes of distributions shift along the temperature increment, and in the area of room temperature, they exist in the infrared region. Thus, it is appropriate to employ infrared measurement for measuring the radiation energy of a blackbody at room temperature.

In following two sections, we describe how we derive the polarization degree in infrared light, by using two approaches. In Section 3.2 we describe how the polarization degree is derived by using Kirchhoff's law from the theory of thermodynamics, and in

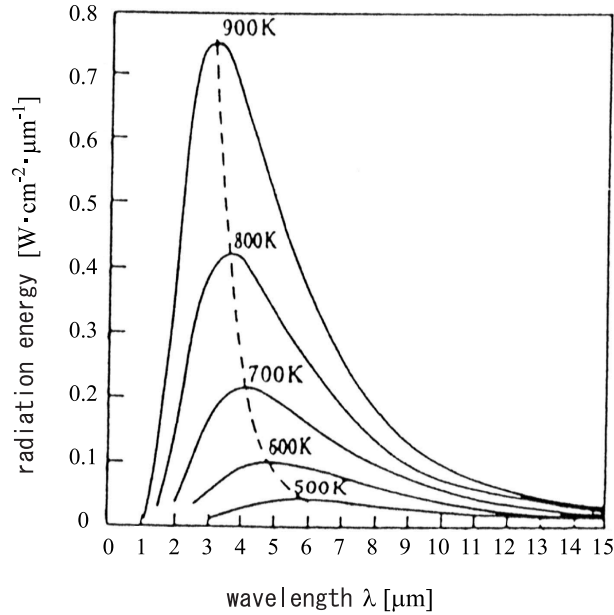


Figure 3.1: Energy distribution of blackbody

Section 3.3 we explain how the polarization degree is derived by considering the light emitted from inside the objects from the theory of optics. As a result, both of the derived polarization degrees will be the same equation.

First, we will describe the unified theory of the polarization in infrared light, which does not depend on whether the object is transparent, translucent, or opaque. To actualize this idea, let us assume that, in a sense, all objects can be considered to be opaque; the light that hits the interface surface of objects can only reflect or be absorbed. The light that transmits into a transparent object will then be referred to as the light that is absorbed into it. The light transmitted into a transparent object escapes into the air from somewhere on the surface of the object. Let us say that such escaped light is the light thermally emitted from the object.

This assumption that all objects can be considered to be opaque is used in Section 3.2. This assumption holds when the corollary is in thermal equilibrium, given that all light is expected to have the same amount of energy and to radiate in all directions.

3.2 Kirchhoff's Law

By considering the state when the corollary is in thermal equilibrium, and by using Kirchhoff's law, we can explain the polarization of thermal radiation[10, 11, 12, 21, 22].

A typical object emits a lower amount of radiation energy than that emitted from a blackbody. The ratio of the amount of radiation energy of a typical object in relation to that from a blackbody is referred to as the emissivity, and is denoted as ε .

Let us assume that infrared light strikes a smooth surface. Its parallel and perpendicular intensity to the plane of incidence are denoted as I_{ap} and I_{as} , respectively. When the infrared light strikes a surface with the incident angle θ , the intensity of parallel and perpendicular components of reflected light are given as $F_p I_{ap}$ and $F_s I_{as}$, respectively.

From the law of the conservation of energy, the difference between the incoming and reflected intensities, $(1 - F_p)I_{ap}$ and $(1 - F_s)I_{as}$, is the amount of energy absorbed by the body. By denoting this ratio as absorptance α , since Kirchhoff's law provides $\varepsilon = \alpha$, we obtain

$$\begin{aligned}\varepsilon_p(T, \lambda, \theta) &= 1 - F_p \\ \varepsilon_s(T, \lambda, \theta) &= 1 - F_s.\end{aligned}\tag{3.2}$$

Let us denote the intensity of thermal radiation from the perfect blackbody as W . Then, the intensity of thermal radiation from our object is εW , and its polarization can be written by using Equation (3.2):

$$\begin{aligned}\rho_{\text{IR}} &= \frac{I_{\text{max}} - I_{\text{min}}}{I_{\text{max}} + I_{\text{min}}} = \frac{\varepsilon_p W - \varepsilon_s W}{\varepsilon_p W + \varepsilon_s W} \\ &= \frac{F_s - F_p}{2 - F_p - F_s}\end{aligned}\tag{3.3}$$

where ρ_{IR} is the polarization degree in infrared light. We use the different notation (i.e. ρ_{IR}) to distinguish this condition from that in the visible light. By substituting Equation (2.1) for Equation (3.3), we can derive the relationship between the polarization degree, ρ_{IR} , and the emitting angle, θ .

3.3 Emitted Light

Let us explain the polarization phenomenon of thermal radiation by considering the light emitted from inside the object [23]. Thermal radiation emitted from inside the object is transmitted through the interface surface and radiated into the air.

For the explanation in this section, suppose material 1 be the object and material 2 be the air, as shown in Figure 2.1. In this case, $\theta_2 > \theta_1$. The refractive index of the object relative to the air will be $n = n_1/n_2$. θ_2 is the emitting angle, and we will derive the polarization degree as a function of $\theta = \theta_2$.

We can define the parallel and perpendicular intensity ratios of transmission, T_p and T_s , as

$$\begin{aligned} T_p &= \frac{I_{tp}}{I_{ap}} = \frac{\sin 2\theta_1 \sin 2\theta_2}{\sin^2(\theta_1 + \theta_2) \cos^2(\theta_1 - \theta_2)} \\ T_s &= \frac{I_{ts}}{I_{as}} = \frac{\sin 2\theta_1 \sin 2\theta_2}{\sin^2(\theta_1 + \theta_2)} \end{aligned} \quad (3.4)$$

where I_{tp} is the component parallel to the X-Z plane of the transmitting light, and I_{ts} is the component perpendicular to the X-Z plane of the transmitting light. Thus, I_{\max} and I_{\min} will be written by using the total energy of the emitted light, W , as

$$I_{\max} = \frac{T_p}{T_p + T_s} W, \quad I_{\min} = \frac{T_s}{T_p + T_s} W. \quad (3.5)$$

By substituting Equation (3.5) and (3.4) into Equation (2.4) with Snell's law, we can represent the degree of polarization of thermal radiation ρ_{IR} as

$$\begin{aligned} \rho_{\text{IR}} &= \frac{I_{\max} - I_{\min}}{I_{\max} + I_{\min}} = \frac{T_p - T_s}{T_p + T_s} \\ &= \frac{(n - 1/n)^2 \sin^2 \theta}{2 + 2n^2 - (n + 1/n)^2 \sin^2 \theta + 4 \cos \theta \sqrt{n^2 - \sin^2 \theta}}. \end{aligned} \quad (3.6)$$

3.4 Polarization Degree of Thermal Radiation

$F_p + T_p = 1$ and $F_s + T_s = 1$ holds, thus the resulting ρ_{IR} in both Section 3.2 (Equation (3.3)) and Section 3.3 (Equation (3.6)) are the same. This is because both explanations deal with the same phenomenon, though the approach is different; one is based on the energy conservation law (Kirchhoff's law), the other on the mechanism of the phenomenon.

Figure 3.2(a) shows the relation between the polarization degree, ρ_{IR} , and the emitting angle, θ .

The refractive index of the graph shown in Figure 3.2(a) is 1.5. Because the refractive index is affected by the wavelength, the refractive index of infrared light is slightly different from that of visible light. For example, the refractive index of glass is approximately 1.52 when the wavelength is approximately 500nm (visible light), and

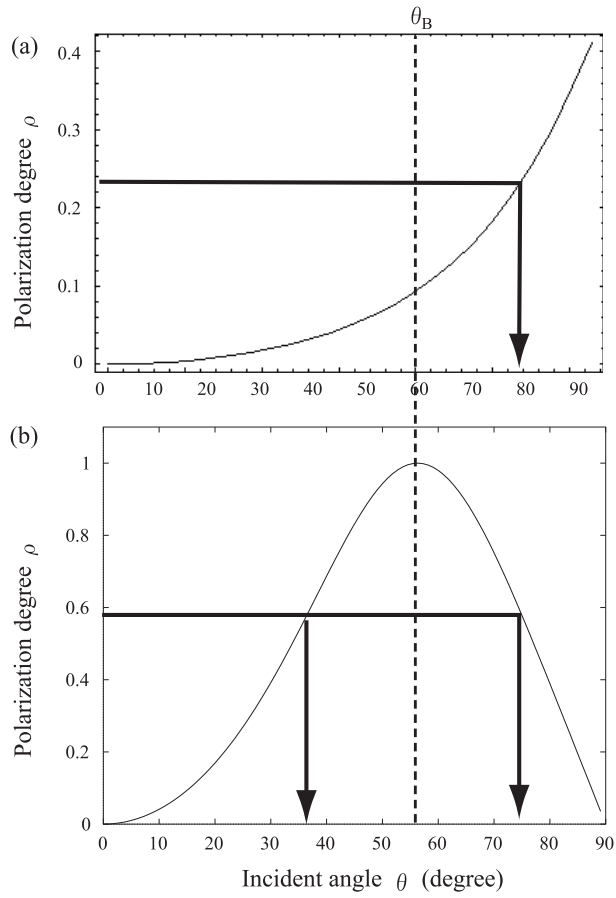


Figure 3.2: Polarization degree of (a)thermal radiation (infrared light) ($n = 1.5$), and (b)reflected light (visible light) ($n = 1.5$)

the refractive index of glass is approximately 1.49 when the wavelength is approximately $2\mu\text{m}$ (infrared light). We use the same refractive index in infrared light as that in visible light because the difference is negligible.

As shown in Figure 3.2(a), the relation is a one-valued function; there is a 1-to-1 correspondence between the polarization degree and the emitting angle. Thus, once we measure the polarization degree in an infrared light, we can uniquely determine the emitting angle. For the sake of comparison, Figure 3.2(b) represents the visible light condition. In this function, as mentioned, one polarization degree corresponds to two emitting angles.

Unfortunately, however, the polarization degree in emitted infrared light is much smaller than that in reflected visible light; at the maximum, around an emitting angle of 90 degrees, it is still 40%. In the smaller area, the polarization degree is less than 10%. In order to obtain such a smaller polarization degree, we are required to measure I_{\max} and I_{\min} precisely. It is impractical to perform such a highly accurate measurement using an ordinary CCD camera with a 256 gray level.

In order to overcome this difficulty, we propose to use both visible and infrared light. By using visible light, we can achieve a highly accurate measurement with ambiguity. By using the infrared light, we discriminate between the two sides. First we determine the polarization degree in the infrared region at the Brewster angle. Using this polarization degree as the threshold value, we can determine to which side, with respect to the Brewster angle, the emitting angle belongs, as indicated by the dotted line in Figure 3.2.

Chapter 4

Object Rotation

In this chapter, we introduce the method of solving the ambiguity by rotating the object.

4.1 Introduction

We explained how to calculate surface normal from polarization data in Chapter 2. In that chapter, we indicated that there exists an ambiguity problem: we cannot uniquely determine the surface normal from several possible surface normals obtained by the measurement. We obtain the incident angle θ ($0^\circ \leq \theta \leq 90^\circ$) and the angle of the incident plane ϕ ($0^\circ \leq \phi < 360^\circ$) from polarization data. Since we define the coordinates as Figure 4.5, the incident angle equals the elevation angle and the angle of the incident plane equals the azimuth angle. Therefore, we can determine the surface normal \mathbf{n} if we obtain two angles θ and ϕ . As we discussed in p.10, we can disambiguate the ambiguity of ϕ ; thus, the problem is to solve the ambiguity of θ . In this chapter, we explain how to disambiguate the ambiguity of θ and to obtain the correct surface normal by rotating the object.

To satisfy this requirement, we propose to tilt (rotate) the object at a small angle. Tilting the object with respect to the camera coincides with observing the object from different directions. We solve the ambiguity by comparing the polarization degree of two data obtained from two different view directions. We have to compare the polarization degree of the two data at the identical point. Namely, we have to find the points of two data which represent the same point on the object surface. For this purpose, we introduce the geometrical property of the object surface. We find some couple of points where the invariant value of the surface is identical, and utilize those

couple of points as matching points.

First of all, we explain the fundamental theory of Gaussian geometry[24, 25], in Section 4.2. Next, we classify some surfaces by the value of curvature (Section 4.3). And, we explain about the definition of “folding point”, in Section 4.4.

In Section 4.5, we segment the data of polarization degree in some regions, and also indicate how we disambiguate each region. We describe the method of finding the matching point by considering geometrical property, in Section 4.6. And, in Section 4.7, we furnish proof that we can obtain the invariant value of geometrical property from the polarization degree data.

Finally, we point out that we can uniquely determine the elevation angle (=incident angle) θ by calculating the difference of the polarization degree between the matching points (Section 4.8).

Consequently, we finally obtain conclusions as follows:

1. We segment the polarization degree data in the B-O region, the B-N region and the B-B region (Section 4.5).
2. We can straightforwardly disambiguate the B-O region and the B-N region as shown in Section 4.5.
3. For the B-B region, we find the point where the polarization degree is minimum and the surface normal is parallel to the rotation direction, and utilize that point as a matching point. We calculate the difference of the polarization degree between those two matching points, and solve the ambiguity from the sign of this difference.

4.2 Gaussian Curvature

We consider that the cross section of the surface S with the plane consists of the unit normal vector \mathbf{n} and the arbitrary unit tangent vector \mathbf{X} at the point P. We call this plane the normal section, and we denote the curve generated by the cross section of the surface and the normal section as c . We represent the curvature of c as $\kappa_{\mathbf{X}}$ (Figure 4.1).

Euler’s theorem

Suppose $\kappa_{\mathbf{X}}$ is not a constant value through the arbitrary unit tangent vector \mathbf{X} at P on S . There exist two unit tangent vectors \mathbf{X}_1 and \mathbf{X}_2 which have the following properties:

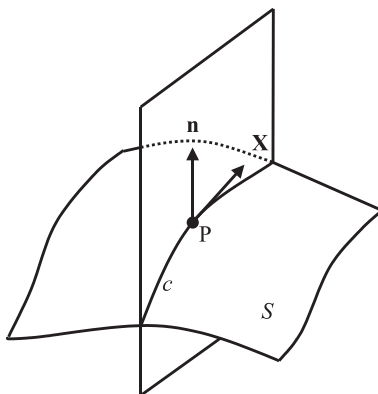


Figure 4.1: Normal section

1. $\kappa_{\mathbf{X}_1}$ is the maximum of $\kappa_{\mathbf{X}}$, $\kappa_{\mathbf{X}_2}$ is the minimum of $\kappa_{\mathbf{X}}$
2. \mathbf{X}_1 and \mathbf{X}_2 are orthogonal.
3. When the angle between \mathbf{X} and \mathbf{X}_1 is represented as ψ ,

$$\kappa_{\mathbf{X}} = \kappa_{\mathbf{X}_1} \cos^2 \psi + \kappa_{\mathbf{X}_2} \sin^2 \psi$$

Definition of principal curvatures

$\kappa_{\mathbf{X}_1}$ and $\kappa_{\mathbf{X}_2}$ are called principal curvatures at the point P, and \mathbf{X}_1 and \mathbf{X}_2 are called principal directions. The plane which consists of \mathbf{n} and \mathbf{X}_1 and the plane which consists of \mathbf{n} and \mathbf{X}_2 , are called principal planes. If $\kappa_{\mathbf{X}_1} = \kappa_{\mathbf{X}_2} = \kappa_{\mathbf{X}}$, the point is called umbilic.

Definition of Gaussian curvature and mean curvature

$K = \kappa_{\mathbf{X}_1} \kappa_{\mathbf{X}_2}$ is called Gaussian curvature at the point P. If P is umbilic ($\kappa_{\mathbf{X}_1} = \kappa_{\mathbf{X}_2} = k$), then $K = k^2$. $H = \frac{1}{2}(\kappa_{\mathbf{X}_1} + \kappa_{\mathbf{X}_2})$ is called mean curvature.

In the following section, we will briefly describe $\kappa_{\mathbf{X}_1}$ as κ_1 and $\kappa_{\mathbf{X}_2}$ as κ_2 .

4.3 Surface Classes

Suppose that we are classifying the surface by Gaussian curvature (Figure 4.2).

We name each class of surface in Figure 4.2 for convenience. From up to down, left to right; elliptic patch, hyperbolic patch, planar patch, cylindrical patch, toric patch, monkeysaddle-shaped patch, slide-shaped patch, and bell-shaped patch. $K > 0$ at

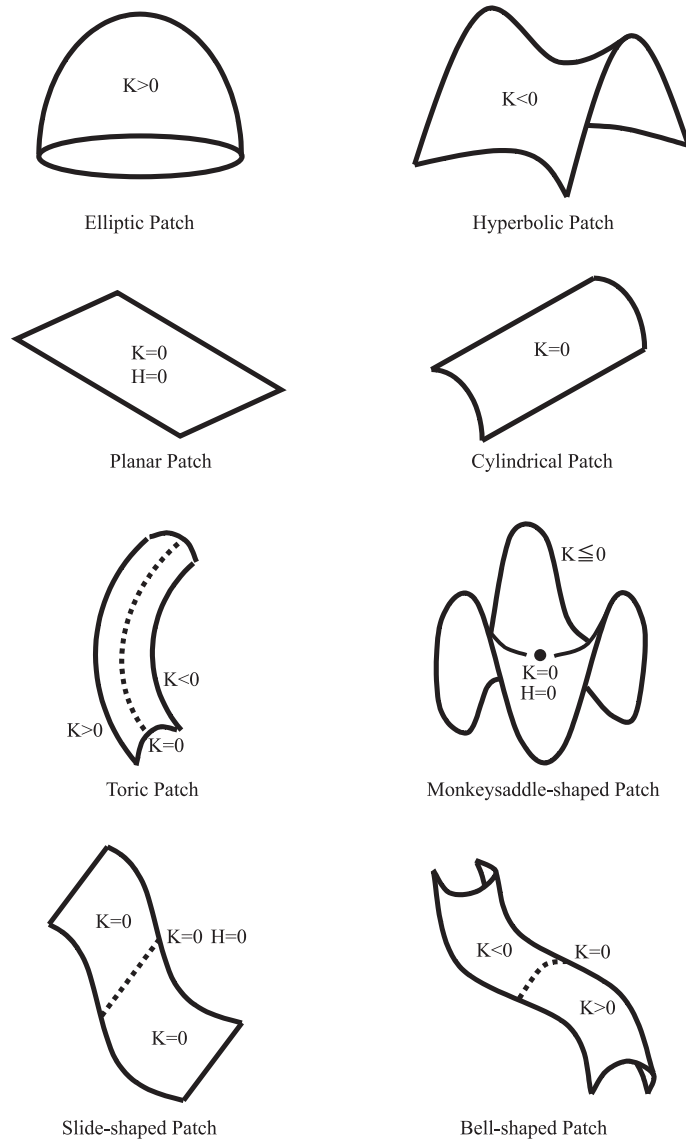


Figure 4.2: Surfaces classified by Gaussian curvature

elliptic patch, $K < 0$ at hyperbolic patch, $K = 0$ at the other patches. We argue the curvatures only at the dotted curve of the toric patch, the slide-shaped patch and the bell-shaped patch, and at the center dot of the monkeysaddle-shaped patch.

The toric patch is shaped like a doughnut, and the Gaussian curvature at the dotted curve is zero. In this figure, the Gaussian curvature of the left part of the dotted curve is positive and that of the right part is negative. The monkeysaddle-shaped patch is shaped like a horse's saddle, but has an additional concave spot to accommodate the monkey's tail. In this figure, the Gaussian curvature at the center dot in the monkeysaddle-shaped patch is zero. The slide-shaped patch is shaped like a children's slide, and the Gaussian curvature is zero at any place. In particular, the dotted line denotes the umbilic point and the principal curvatures are zero. The slide-shaped patch consists of two cylindrical patches stuck at the dotted line. The bell-shaped patch is shaped like a part of a bell, and the Gaussian curvature of the dotted curve is zero. In this figure, the Gaussian curvature of the upper part of the dotted curve is negative and that of the lower part is positive.

Surfaces can be classified in three types, $K > 0$, $K < 0$ and $K = 0$, but we consider the more detailed classification of each surfaces in Figure 4.2 by the sign of κ_1 , κ_2 ($\kappa_1 > \kappa_2$). The Gaussian curvature K , mean curvature H , and principal curvatures κ_1 and κ_2 of each surfaces in Figure 4.2 are shown in Table 4.1. Note that the curvatures of the toric patch, the slide-shaped patch and the bell-shaped patch described in this table are the curvatures at the dotted curve of those patches, and the curvatures of the monkeysaddle-shaped patch are the curvatures at the center dot.

4.4 Folding Point

In Figure 4.3, we describe the relationship between the shapes of the 1D curve represented on 2D plane and their curvatures.

The shape of the curve is represented as $h = f(t)$ and depicted in Figure 4.3(a). Figure 4.3(b) shows the elevation angle θ of each point on the curve. Figure 4.3(c) represents the Gaussian mapping from the normal of the curve to the unit circle (Gaussian circle).

The curve convex to the upper direction described in the topmost row has positive curvature, the curve convex to the lower direction described in the second row has negative curvature, and the curve described in the rows below the second row has zero curvature. As denoted in the rows below the second row, there are two classes of curves whose curvature will be zero; one is a line, the other is an inflection point.

Surface classes	Possible combinations of curvatures		
Elliptic patch	$K > 0, H > 0,$ $\kappa_1 > 0, \kappa_2 > 0$	$K > 0, H < 0,$ $\kappa_1 < 0, \kappa_2 < 0$	
Hyperbolic patch	$K < 0, H < 0,$ $\kappa_1 > 0, \kappa_2 < 0$	$K < 0, H = 0,$ $\kappa_1 > 0, \kappa_2 < 0$	$K < 0, H > 0,$ $\kappa_1 > 0, \kappa_2 < 0$
Planar patch	$K = 0, H = 0,$ $\kappa_1 = 0, \kappa_2 = 0$		
Cylindrical patch	$K = 0, H > 0,$ $\kappa_1 > 0, \kappa_2 = 0$	$K = 0, H < 0,$ $\kappa_1 = 0, \kappa_2 < 0$	
Toric patch	$K = 0, H > 0,$ $\kappa_1 > 0, \kappa_2 = 0$	$K = 0, H < 0,$ $\kappa_1 = 0, \kappa_2 < 0$	
Monkeysaddle-shaped patch	$K = 0, H = 0,$ $\kappa_1 = 0, \kappa_2 = 0$		
Slide-shaped patch	$K = 0, H = 0,$ $\kappa_1 = 0, \kappa_2 = 0$		
Bell-shaped patch	$K = 0, H > 0,$ $\kappa_1 > 0, \kappa_2 = 0$	$K = 0, H < 0,$ $\kappa_1 = 0, \kappa_2 < 0$	

Table 4.1: Surface classes and curvatures

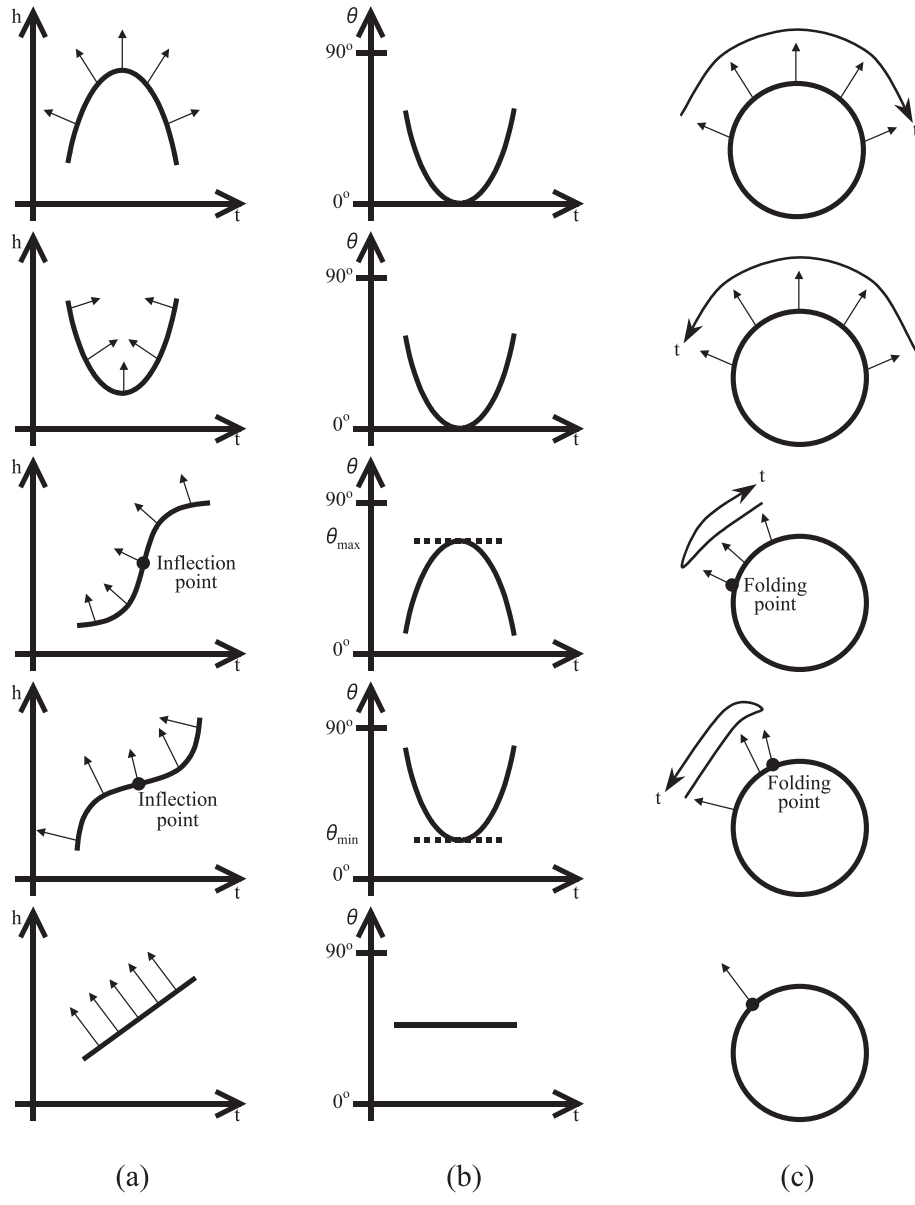


Figure 4.3: Curves classified by curvature. (a) Shape of curves. (b) Elevation angle of (a). (c) Gaussian circle of (a).

By examining at the graph of the elevation angle θ at the inflection point (Figure 4.3(b)), we determine that the elevation angle θ is locally maximum or locally minimum at the inflection point. If an elevation angle θ is locally maximum at a certain point, there is no larger angle than the local maximum θ_{\max} in the neighboring points. In this case, when we track the point on the Gaussian circle along t , the direction of the tracking reverses at a certain point. If an elevation angle θ is locally minimum at a certain point, there is no smaller angle than the local minimum θ_{\min} in the neighboring points. In this case, when we track the point on the Gaussian circle along t , the direction of the tracking reverses at a certain point. We define the “folding point” as an inflection point.

We will adopt a similar definition for the 2D surface represented in 3D space. We define the “folding point” as an inflection point of the curve generated by the cross section of the surface and the arbitrary plane which includes the surface normal.

Let us see if there appear a folding point in each surface classes described in Section 4.3. The folding point never appears unless the Gaussian curvature is zero. Figure 4.4 represents an example of the Gaussian mapping to the Gaussian sphere from the planar patch, the cylindrical patch, the toric patch, the monkeysaddle-shaped patch, the slide-shaped patch, and the bell-shaped patch.

The planar patch is mapped onto a point on the Gaussian sphere, and the cylindrical patch is mapped onto a curve on the Gaussian sphere. The toric patch is mapped onto an image which is point symmetry to a certain point. The point where $K = 0$ is mapped onto that point on the Gaussian sphere. If we track from the point where $K < 0$ to the point where $K > 0$, we pass through the point where $K = 0$. The points where $K = 0$ are not folding points. The monkeysaddle-shaped patch has a folding point which is denoted in the figure as the dot in the center of the patch ($K = 0$ and $H = 0$). The slide-shaped patch also has folding points which are denoted in the figure as a dotted line ($K = 0$ and $H = 0$). The bell-shaped patch has folding points which are denoted in the figure as a dotted curve ($K = 0$).

We use the term “folding curve” to denote the curve which consists of folding points.

For the bell-shaped patch in this figure, the upper surface where $K < 0$ and the lower surface where $K > 0$ are mapped onto the southern part from the folding curve, where $K = 0$. If the point walks from the point where $K > 0$ to the point where $K < 0$, the point walks on the Gaussian sphere first from south to north, and then arrives at the folding curve when $K = 0$; the point then turns in the opposite direction, and walks from north to south.

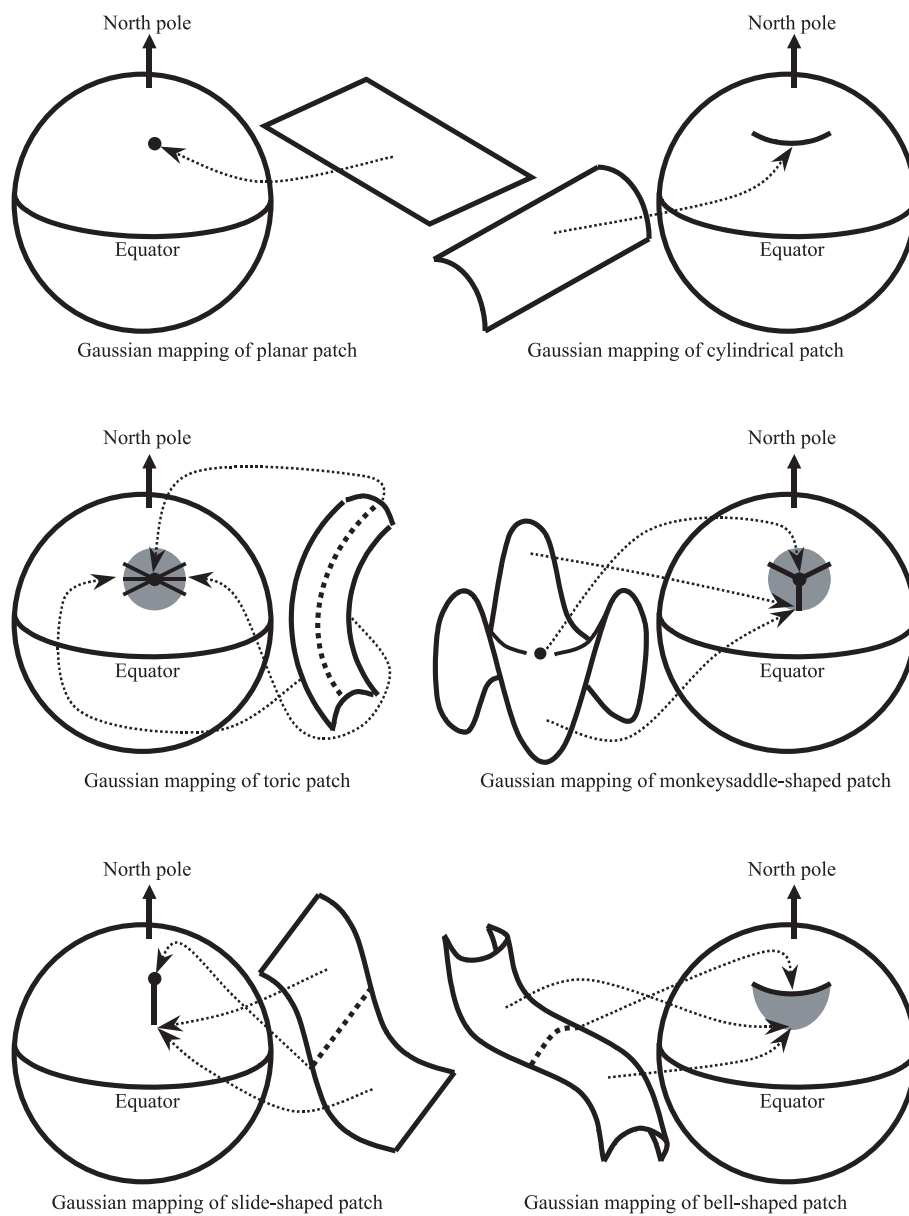


Figure 4.4: Gaussian mapping of some patches

Two lines appear in the principal directions for a planar patch. A convex curve and a line appear in the principal directions for a cylindrical patch. A convex curve and a line appear in the principal directions at the point where $K = 0$ for a toric patch. Either a line and an inflection point, or two inflection points, or two lines appear in the principal directions at the point where $K = 0$ and $H = 0$ for a monkeysaddle-shaped patch. A line and an inflection point or two inflection points appear in the principal directions at the point where $K = 0$ and $H = 0$ for a slide-shaped patch. A convex curve and an inflection point appear in the principal directions at the point where $K = 0$ for a bell-shaped patch.

4.5 Brewster Segmentation

We explained how to obtain the polarization degree of the light reflected on the object surface in Chapter 2. Now we segment the data of polarization degree into some regions bounded by Brewster angle θ_B . Points of Brewster angle have no ambiguity and the polarization degree ρ is equal to 1.

We assume that the object is projected orthographically to the camera. In addition, we assume that the surface shape observed from the camera causes no self occlusion; thus, the surface is a regular surface and can be represented as $z = f(x, y)$.

Also we assume that the object surface is sufficiently smooth (2 or 3 times differentiable). From these assumptions, the curve connected with points where the elevation angle is Brewster angle will form a closed curve. We denote a point where the elevation angle is equal to Brewster angle as the ‘‘Brewster point,’’ and the closed curve consisting of Brewster points as the ‘‘Brewster curve’’. We define the segmentation by Brewster curves as ‘‘Brewster segmentation’’.

Now we want to determine the incident angle (elevation angle) θ ; however, the correspondence between the polarization degree ρ and the incident angle θ is 1 to 2; thus, we have to disambiguate this ambiguity to determine the correct incident angle (Figure 2.3). The incident angle of all points in the region segmented through the Brewster segmentation, is either greater than the Brewster angle or smaller than the Brewster angle. Therefore, we can uniquely determine all the incident angles in the region if we can disambiguate only one point in the region. The graph described in Figure 2.3 indicates that the correspondence between θ and ρ is 1 to 1 at $0^\circ \leq \theta \leq \theta_B$, and also 1 to 1 at $\theta_B \leq \theta \leq 90^\circ$ (details are written in p.36). Therefore, if we know whether the incident angle θ is greater or smaller than Brewster angle θ_B , we can determine the value of θ uniquely from the value of ρ .

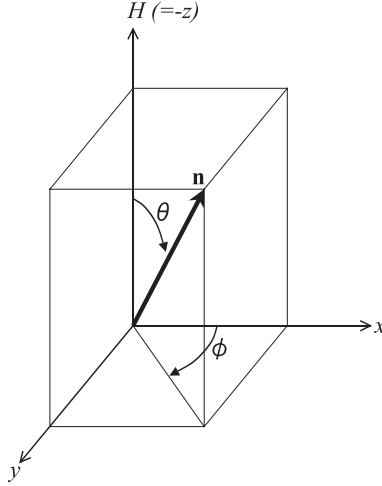


Figure 4.5: Coordinates of surface normal

The coordinates are defined as Figure 4.5, where the camera is placed at the $H = (-z)$ axis. We define θ as the angle between surface normal and H axis, ϕ as the angle, from x axis to y axis, between x axis and the projected vector of surface normal to x - y plane. Therefore, the incident angle θ ($0^\circ \leq \theta \leq 90^\circ$) represents the elevation angle of the surface normal \mathbf{n} , and the angle of the plane of incidence ϕ ($0^\circ \leq \phi < 360^\circ$) represents the azimuth angle of the surface normal \mathbf{n} .

Regions are grouped into three classes, which we will denote as follows;

1. B-O region
2. B-N region
3. B-B region

‘B’ represents the capital letter of Brewster curve, ‘O’ represents the capital letter of Occluding boundary, and ‘N’ represents the capital letter of North pole. North pole is that of the Gaussian sphere, the direction where the camera is placed.

The polarization degree of the points of the Brewster curve is 1; thus, there is no ambiguity and the elevation angle (incident angle) θ can be determined uniquely. The surface normal of the points of occluding boundary faces out from the object and is perpendicular to the view direction, and the elevation angle θ is 90° . There exist no data outside the occluding boundary. The elevation angle θ of the points which maps onto the north pole is 0° , while, the angle of the plane of incidence (the azimuth angle)

ϕ is undefined at those points. Therefore, segmenting regions by B-curve, O-curve, and N-curve is considered to be the most efficient segmentation.

B-O region is the region which includes the occluding boundary. B-N region is the region which includes the points which can be mapped onto the north pole of Gaussian sphere. B-B region is the region which includes neither the occluding boundary nor the north pole points, and is bounded only by Brewster curves.

We assume that, even if we tilt the object in an infinitesimal angle in any direction, the class of the region never changes through such object rotations. Specifically, we assume that the number of regions does not change through any object rotations, and also that each regions deform and translate only infinitesimally. In addition, we assume that the self-occlusion never occurs even if we were to tilt the object at an infinitesimal angle.

To satisfy the above assumptions, we consequently assume that there are no points where the elevation angle θ is equal to 90° except for the occluding boundary. Therefore, the only region which has the points where the elevation angle θ is equal to 90° is B-O region, and there are no regions which have the points where the elevation angle θ is equal to 90° except for B-O region. As a result, if there is a point where the polarization degree ρ equals to 0, the elevation angle θ of that point always be 0° except for the occluding boundary. B-N region is defined to have a point where the elevation angle θ equals to 0° ; thus, only the B-N region has a point where the polarization degree ρ equals to 0 except for B-O region. We defined that the region which is neither B-O region nor B-N region is the B-B region; thus, the elevation angle θ of the points in B-B region equals to neither 0° nor 90° .

By calculating the background subtraction image, the occluding boundary can be calculated; thus, the B-O region is easily determined. The B-N region is determined only by searching the point where the polarization degree equals zero. The region which is neither the B-O region nor the B-N region is the B-B region. Therefore, the obtained data of polarization degree can be easily classified into B-O region, B-N region, and B-B region even if we do not solve the ambiguity.

B-O region includes the occluding boundary whose elevation angle θ equals to 90° ; thus, we can disambiguate this region and determine the elevation angle to be in the range of $\theta_B \leq \theta \leq 90^\circ$. B-N region includes the points that will be mapped onto the north pole of the Gaussian sphere, whose elevation angle θ equals to 0° ; thus, we can disambiguate this region and determine the elevation angle to be in the range of $0^\circ \leq \theta \leq \theta_B$. In the following sections, we will discuss only the method of disambiguating B-B regions.

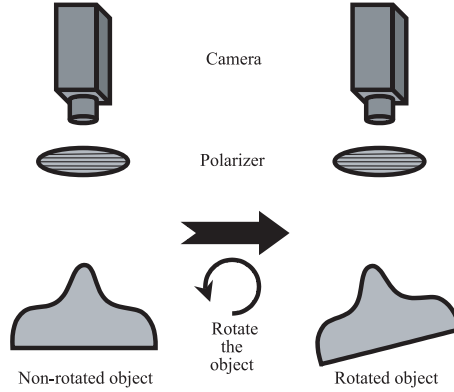


Figure 4.6: Object rotation

4.6 Matching Point

We obtain one set of data of the polarization degree for input data. However, one set of data is not enough for disambiguating the ambiguity in the B-B region; thus, we obtain extra data. We tilt (rotate) the object in a small angle and obtain another additional data of polarization degree (Figure 4.6).

We will solve the ambiguity in the B-B region by comparing the data of the polarization degree of the object placed unrotated and that of the object rotated at a small angle. For comparison, we should find identical points (matching points) of two data of polarization degree. By adopting the geometrical property of the object surface, we investigate an invariant property of the object surface unchangeable through the object rotation. We compare the polarization degree at two points where the invariant property on the surface matches, and disambiguate the ambiguity problem. We adopt the “folding point” (Section 4.4) for this invariant property of object surface.

The Gaussian mapping of the B-B region of the object surface onto the Gaussian sphere is depicted in Figure 4.7. The B-B region includes neither the occluding boundary nor the north pole point, and is bounded only by the Brewster curve; thus, the folding curve always appears.

Because curvature is a property of a surface, it is an invariant value which is not changed by rotating the object. For this reason, considering curvatures for finding matching points is a suitable option. It is better to adopt a point where the curvature is zero rather than the curvature itself, because the curvature can be easily influenced by an error and has ambiguity. Therefore, we adopt folding curves. Adoption of

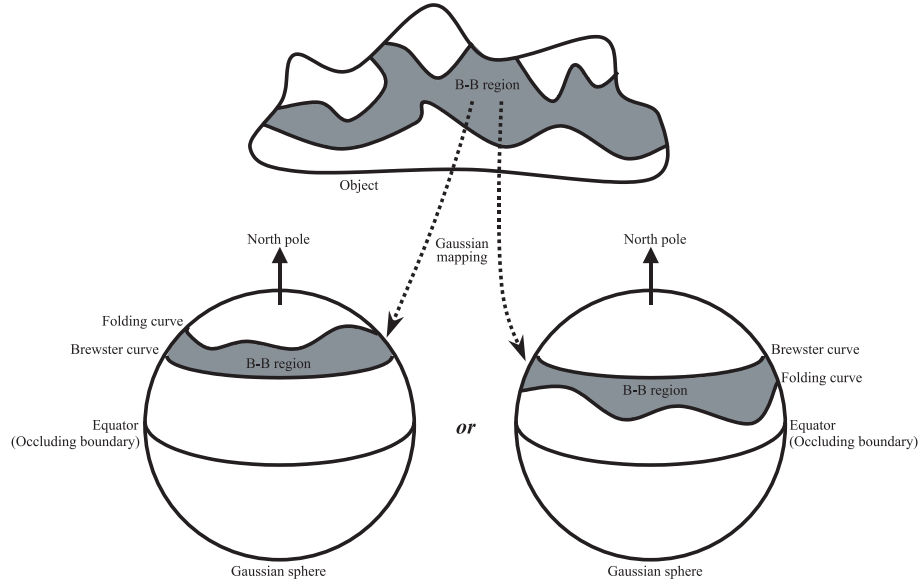


Figure 4.7: Gaussian mapping of B-B region

folding curves is the most practical idea, because folding curves always appear in the B-B region.

We cannot determine the number of folding curves that will appear in a closed region; however, we can state that the boundary of the region in the Gaussian sphere which is not the Brewster curve is always a folding curve. Therefore, we utilize the boundary of the region of the Gaussian sphere mapped from B-B region (=folding curve) for the matching. Namely, if the B-B region is to the north of Brewster curve, we utilize the northernmost folding curve for the matching; and if the B-B region is to the south of the Brewster curve, we utilize the southernmost folding curve for the matching.

However, there is a problem in matching two folding points. We can decide which folding curve corresponds to which folding curve, but we cannot decide which point on the folding curve corresponds to which point on the folding curve. Therefore, we define the matching point as the point where the folding curve and the great circle intersect (Figure 4.8). This great circle must be a cross-section between the Gaussian sphere and the plane which is parallel to the rotation direction of the object and includes the north pole of the Gaussian sphere. The surface point which is mapped onto this great circle, still maps onto this great circle after the object rotation, thus enabling unique

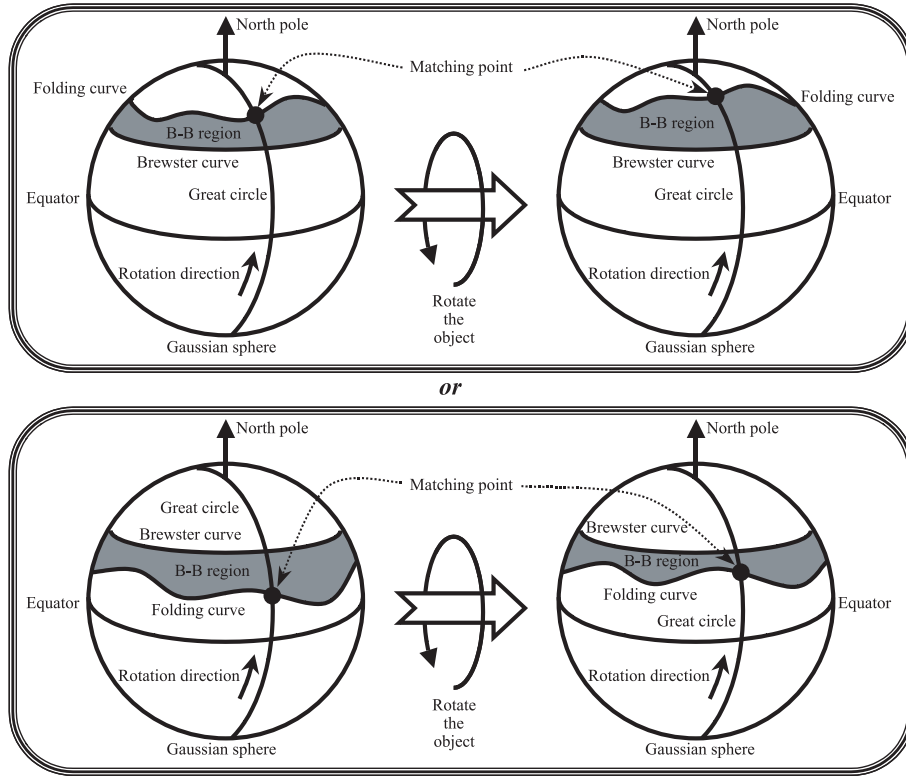


Figure 4.8: Matching Point

matching.

Summary:

1. If the B-B region is mapped onto the north of the Brewster curve, choose the northernmost point for the matching point which intersects the great circle; namely, choose the point where the polarization degree is minimum.
2. If the B-B region is mapped onto the south of the Brewster curve, choose the nearest point to the equator for the matching point which intersects the great circle; namely, choose the point where the polarization degree is minimum.

There exist one or two points where the polarization degree is minimum and where the folding curve and the great circle intersect. If there are two points, we can distinct those points, because the azimuth angle ϕ is in direct opposition; thus, there is no difficulty for matching.

Our conclusion is that the point of the B-B region where the polarization degree is minimum and the surface normal lies along the rotation direction is the best matching point to adopt (Figure 4.8).

There is not always only one point of the surface which maps onto the matching point on the Gaussian sphere. For instance, there are several points which fit the above definition of matching point in the slide-shaped patch shown in Figure 4.2. However, our aim is a comparison of the value of polarization degree in two points, not matching at two points (see Section 4.8 for more detail). There exist many points on the surface which fit the above definition of matching point; however, the value of the polarization degree does not change even if we choose any matching point. Therefore, even though there are several matching points, the disambiguating process will not be disturbed.

4.7 Folding Point of Polarization Degree

It is apparent by looking at the figure that a folding curve of elevation angle θ is also a folding curve of polarization degree ρ . In this section, however, we will prove this fact algebraically.

We denote the position of the point of the curve on the surface as s . The value of the elevation angle θ of the point on the surface is a function of s . The conditions which elevation angle θ be the maximum are;

$$\frac{d\theta}{ds} = 0 \quad \text{and} \quad \frac{d^2\theta}{ds^2} < 0 \quad . \quad (4.1)$$

The conditions which elevation angle θ be the minimum are;

$$\frac{d\theta}{ds} = 0 \quad \text{and} \quad \frac{d^2\theta}{ds^2} > 0 \quad . \quad (4.2)$$

If the polarization degree ρ satisfies the following, it will be the minimum.

$$\frac{d\rho}{ds} = 0 \quad \text{and} \quad \frac{d^2\rho}{ds^2} > 0 \quad . \quad (4.3)$$

The derivative of the polarization degree ρ by the elevation angle θ (see Equation (4.13) & Figure 4.9 for more detail) have the following nature;

$$\frac{d\rho}{d\theta} > 0 \quad (0^\circ < \theta < \theta_B) \quad (4.4)$$

$$\frac{d\rho}{d\theta} < 0 \quad (\theta_B < \theta \leq 90^\circ) \quad (4.5)$$

$$\frac{d\rho}{d\theta} = 0 \quad (\theta = 0^\circ \quad \text{or} \quad \theta = \theta_B) \quad . \quad (4.6)$$

We are now considering the points in B-B region; thus, θ never equals 0° . And also, we are not considering the points on the Brewster curve (=boundary of the region); thus, we can claim that the elevation angle θ does not coincide with the Brewster angle θ_B . Therefore, $d\rho/d\theta \neq 0$.

The first and second derivatives of the polarization degree ρ by arbitrary axis s are as follows;

$$\frac{d\rho}{ds} = \frac{d\rho}{d\theta} \frac{d\theta}{ds} \quad (4.7)$$

$$\frac{d^2\rho}{ds^2} = \frac{d^2\rho}{d\theta^2} \left(\frac{d\theta}{ds}\right)^2 + \frac{d\rho}{d\theta} \frac{d^2\theta}{ds^2} \quad (4.8)$$

First, the $\theta < \theta_B$ case, which the B-B region mapped onto the Gaussian sphere is to the north of Brewster curve. In this case, the elevation angle θ is minimum at the folding curve. From Equation (4.2), (4.4), (4.7) and (4.8), the first and second derivatives of the polarization degree ρ by s at this point will be as follows;

$$\begin{aligned} \frac{d\rho}{ds} &= 0 \\ \frac{d^2\rho}{ds^2} &= \frac{d\rho}{d\theta} \frac{d^2\theta}{ds^2} > 0 \end{aligned} \quad (4.9)$$

Therefore, considering Equation (4.3), the polarization degree ρ is minimum as expected.

Next, the $\theta > \theta_B$ case, which the B-B region mapped onto the Gaussian sphere is to the south of the Brewster curve. In this case, the elevation angle θ is maximum at the folding curve. From Equation (4.1), (4.5), (4.7) and (4.8), the first and second derivatives of the polarization degree ρ by s at this point will be as follows;

$$\begin{aligned} \frac{d\rho}{ds} &= 0 \\ \frac{d^2\rho}{ds^2} &= \frac{d\rho}{d\theta} \frac{d^2\theta}{ds^2} > 0 \end{aligned} \quad (4.10)$$

Therefore, considering Equation (4.3), the polarization degree ρ is minimum as expected.

First, we proved that, at the folding curve of northernmost elevation angle θ , the polarization degree ρ is also a folding curve, when the B-B region is mapped onto the north of the Brewster curve on the Gaussian sphere. Next, we proved that, at the folding curve of southernmost elevation angle θ , the polarization degree ρ is also a folding curve, when the B-B region is mapped onto the south of the Brewster curve on the Gaussian sphere.

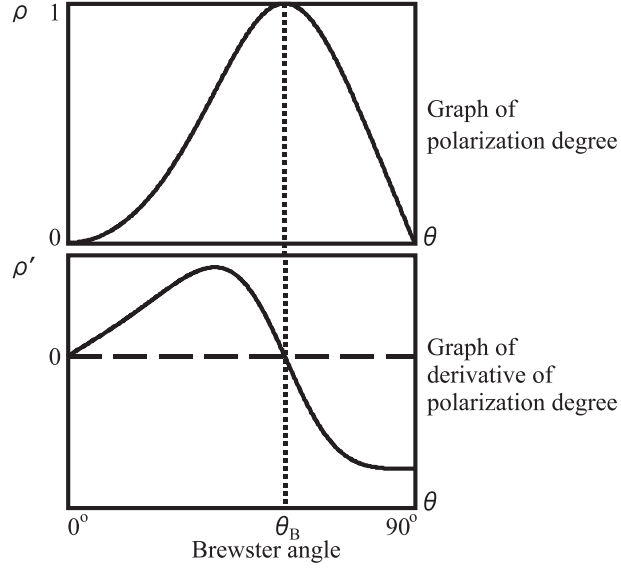


Figure 4.9: Graph of derivative of polarization degree.

4.8 Difference of Polarization Degree

Finally, we explain the method to disambiguate the ambiguity problem of the surface normal by comparing the polarization degree at the matching point of the object which is not tilted with that of the object which is tilted at a small angle.

We regard the refractive index n as constant; thus, the polarization degree ρ is only a function of the elevation angle θ . If the rotation angle is $\delta\theta$, the Taylor expansion of the polarization degree $\rho(\theta + \delta\theta)$ around θ will be;

$$\rho(\theta + \delta\theta) = \rho(\theta) + \rho'(\theta)\delta\theta + O((\delta\theta)^2) \quad . \quad (4.11)$$

Therefore, if $\delta\theta$ is sufficiently small, the difference of two polarization degrees will be;

$$\rho(\theta + \delta\theta) - \rho(\theta) = \rho'(\theta)\delta\theta \quad . \quad (4.12)$$

The derivative of the polarization degree ρ by the elevation angle θ is;

$$\frac{d\rho}{d\theta} = \frac{2 \sin \theta (n^2 - \sin^2 \theta - n^2 \sin^2 \theta) (2n^2 - \sin^2 \theta - n^2 \sin^2 \theta)}{\sqrt{n^2 - \sin^2 \theta} (n^2 - \sin^2 \theta - n^2 \sin^2 \theta + 2 \sin^4 \theta)^2} \quad . \quad (4.13)$$

The graph of this equation is depicted in Figure 4.9.

The derivative of the polarization degree $d\rho/d\theta$ is positive when $0^\circ < \theta < \theta_B$, and is negative when $\theta_B < \theta \leq 90^\circ$.

We do not need to know the rotation angle; however, we assume that we know the rotation direction. And of course, the azimuth angle ϕ has already been determined. Therefore, we can determine the sign of $\delta\theta$. As a result, by calculating the sign of the difference of two polarization degrees at the matching point using Equation (4.12), and from the sign of that difference, we can determine whether the elevation angle θ is greater or less than the Brewster angle.

Consequently, we can determine whether the elevation angle θ in B-B region is in the range of $0^\circ \leq \theta \leq \theta_B$ or $\theta_B \leq \theta \leq 90^\circ$.

And we can also see from Figure 4.9 that the polarization degree ρ is an increasing function in the range of $0^\circ \leq \theta \leq \theta_B$ and is a decreasing function in the range of $\theta_B \leq \theta \leq 90^\circ$. Namely, the correspondence between the polarization degree ρ and the elevation angle θ is 1 to 1 in the range of $0^\circ \leq \theta \leq \theta_B$, and also is 1 to 1 in the range of $\theta_B \leq \theta \leq 90^\circ$. Therefore, if we just determine that the elevation angle θ in B-B region is whether in the range of $0^\circ \leq \theta \leq \theta_B$ or $\theta_B \leq \theta \leq 90^\circ$, we can determine the elevation angle θ uniquely from the value of the polarization degree ρ .

Chapter 5

Experiments

5.1 Experimental Setup

5.1.1 Experimental Setup of Visible Light

Figure 5.1(a) shows the apparatus for visible light measurement. As a light source, we employ a spherical diffuser illuminated from point light sources. This spherical diffuser becomes a secondary light source and illuminates an object that is located at the center of the sphere from all directions. Because we determine surface orientations using only surface reflection and the surface reflection occurs only when the emitting and incident angles are the same, it is necessary to illuminate an object from all directions in order to observe surface reflections over the entire object surface.

We use three 300W incandescent light bulbs as the point sources, located circularly and at 120 degrees apart. The spherical diffuser is made of plastic and its diameter is 40 cm. The object, as mentioned above, is located at the center of the sphere, and is illuminated by this spherical diffuser, which works as an unpolarized spherical light source. This object is observed through a small hole at the top of the sphere by a black and white CCD camera. A polarization filter is mounted between the hole and the TV camera.

5.1.2 Experimental Setup of Infrared Light

Figure 5.1(b) shows the apparatus for the infrared light. Given that the infrared light is thermal radiation from a body and is not a reflection component, we do not use any light source. Any object emits infrared light. However, at room temperature, the amount of infrared light emitted from the object in 3-5 μm is relatively small, and

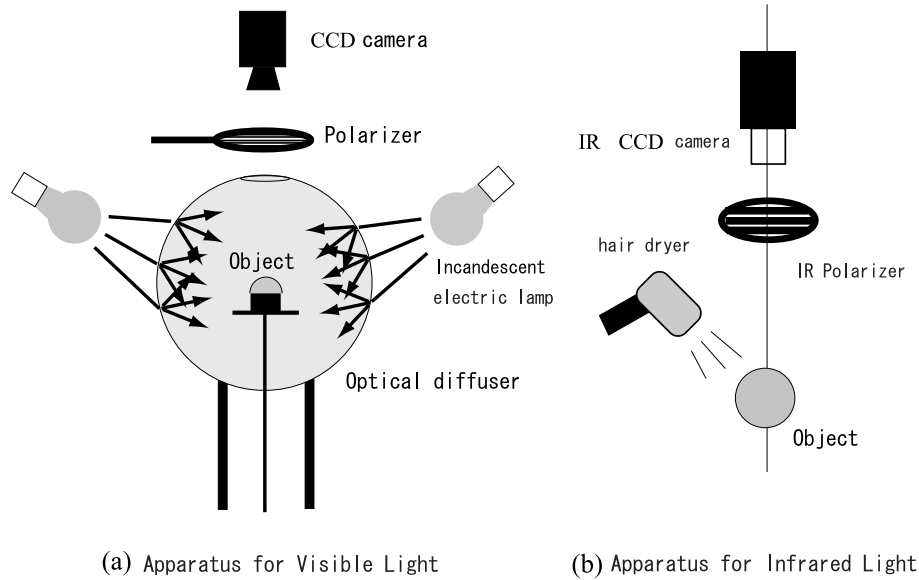


Figure 5.1: Experimental setup

contains infrared light emitted from the air. This makes the measurement of I_{\max} and I_{\min} very sensitive to noise. Thus, we increase the temperature of the object to 30-40 degrees Celsius, and subtract that from the air temperature to obtain the amount of infrared light emitted solely from the object.

In order to increase the temperature of the object, we use a hair dryer to blow heated air over it. We also employ an infrared filter and an IR-CCD camera in 3-5 μm . Our IR-CCD camera determines an appropriate gain in order to map the temperature range onto a 256 gray level. Thus, a measured intensity is converted to a temperature. In order to determine the polarization degree, we convert the measured temperature into intensity using Equation (3.1).

5.2 Measurement

5.2.1 Measurement of Non-rotated Object in Visible Light Domain

By rotating a polarization filter, we obtain a sequence of images of an object. We measure from 0 degrees through 175 degrees at 5 degree intervals. From this process we obtain 36 images.

At each pixel of the 36 images, we observe variance of intensity and determine the maximum and minimum intensities, I_{\max} and I_{\min} . Because those measurements occur at 5 degree intervals, it is difficult to obtain the exact maximum and minimum values. By using the least square minimization, we fit a sinusoidal curve to those obtained measurements, then determine the maximum and minimum values. From those values, we determine two possible surface orientations using the algorithm.

5.2.2 Measurement of Thermal Radiation

For the infrared measurement, we heat the object to a temperature of 30-40 degrees Celsius by using the hair dryer for a certain period. Once equilibrium in the heat exchange is achieved, we use the same procedure, rotating the polarization filters and obtaining a sequence of images, as we did in the visible light measurement. Here, the maximum and minimum correspond to T_{\max} and T_{\min} ; we convert them to I_{\max} and I_{\min} as appropriate, then obtain the polarization degree.

After the measurements in infrared and visible light, we compare those data at each pixel. For alignment, we use two calibration points around the object; by extracting these two points in both image sequences, we can align the two measurements. At each pixel, measurement in visible light provides two solutions. Then, from the polarization degree in infrared measurement, we can choose one of the solutions; it is determined whether the obtained polarization degree in infrared light is smaller or larger than the infrared polarization degree at the Brewster's angle, ρ_{IR}^* .

5.2.3 Measurement of Rotated Object

First, we use the same procedure, rotating the polarization filters and obtaining a sequences of images, as we did for the non-rotated object.

Next, we apply the same measurement to the rotated object. The object is rotated slightly to make a novel view observed from the fixed camera. After the same calculation, we obtain the polarization degree of this second view.

After obtaing those measurements, we compare the measurements of those two data at each corresponding point. To determine the corresponding points of the two data, we first separate the polarization data into some regions by the Brewster angle. Then, we detect a minimum value of the polarization degree in each region whose surface normal is the same orientation as the rotating direction. Finally, the difference value of the polarization degrees in those two corresponding points disambiguates the problem of the ambiguity of the angle; as a result, we obtain the correct incident angle of the object surface.

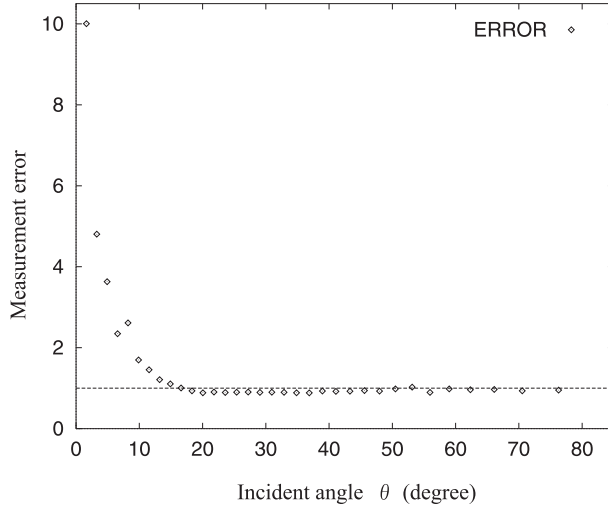


Figure 5.2: Error characteristics of the spherical object

5.3 Experimental Result

5.3.1 Experimental Result of Thermal Radiation Method

Experiments using a spherical object

In order to determine the accuracy of the system, we use an acrylic sphere having a refractive index of 1.5 and a diameter of 5cm. Figure 5.2 shows the error characteristics from the observed measurement. The horizontal axis is the emitting angle and the vertical axis denotes the measurement errors. In the figure, the dotted straight line denotes the case without any measurement errors.

From this experiment, except around the area of small angles, the measurement error is small and we can achieve high accuracy in measurement.

One of the reasons for the relatively noisy data around the smaller angles is that the spherical diffuser has a hole in its top portion, and the object does not receive light from that area. Another reason is that the derivative of the degree of polarization is close to zero where the incident angle is near 0° , and is less stable for determining the incident angle from the degree of polarization.

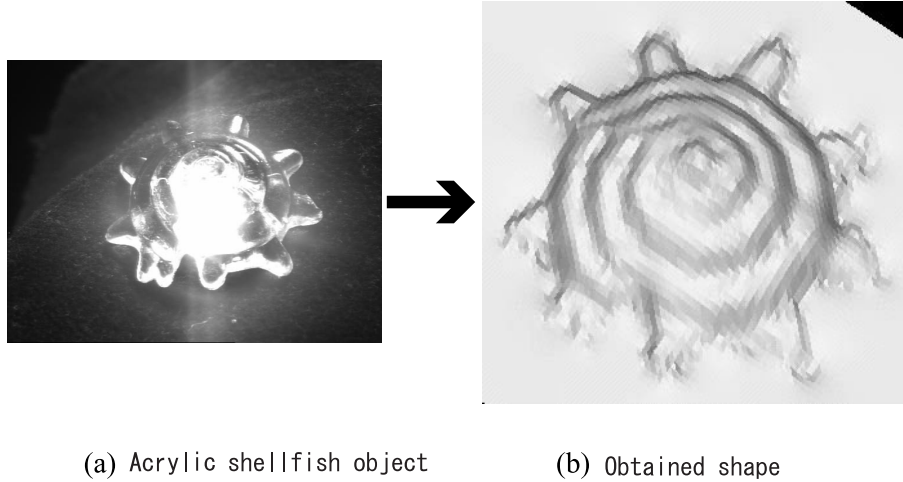


Figure 5.3: The resulting shape of the shellfish-shaped object

Experiments using a shellfish-shaped object

In order to demonstrate the applicability of our system to an object of general shape, we determined the shape of the object shown in Figure 5.3(a). The shellfish-shaped object is made of acrylic and its refractive index is 1.5. Figure 5.3(b) shows the obtained shape of the object. Here the system provides the distribution of surface orientations. From this obtained distribution, a relaxation algorithm [26] converts the orientation distribution into a shape corresponding to that of the object.

Figure 5.3(b) recovers the original shape. Notably, the area of steeper angles (i.e., those larger than the Brewster angle) provides better recovery results. At the boundary, the shape is a bit noisy. At that region, the polarization degree is almost zero, and it is difficult to determine this value.

5.3.2 Simulational Result of Object Rotation Method

Before practicing our object rotation method, we applied our technique to simulation objects to verify the effectiveness of our method. Figure 5.4, 5.5, and 5.6 is the result of the simulation. Figure 5.4(a), 5.5(a), and 5.6(a) depict Brewster curves and occluding boundary of simulation objects. There are 5, 6, and 3 regions depicted in Figure 5.4(a), 5.5(a), and 5.6(a), respectively. Figure 5.4(b), 5.5(b), and 5.6(b) depict the result 3D shapes. Our simulation software produces the data of polarization degree, and our disambiguating software computes the surface normal of the object. In this

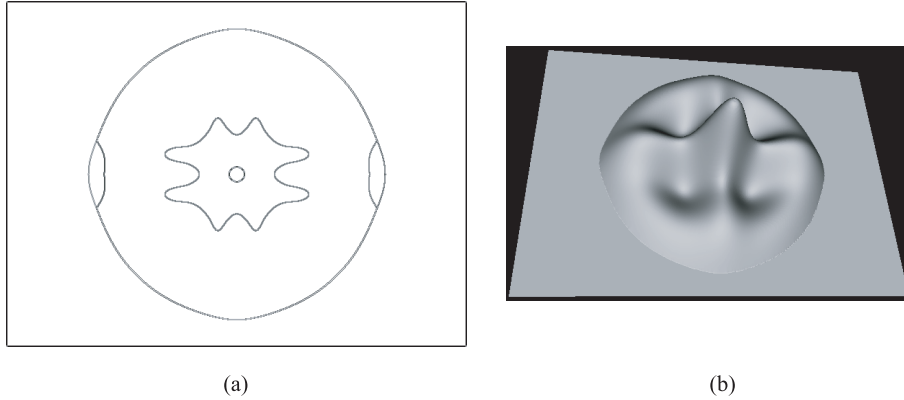


Figure 5.4: Simulation result of the object No.1. (a) Boundaries of each regions. (b) The result 3D-shape.

simulation, we inspected the effectiveness of our method which solves the ambiguity and determined the correct incident angle, θ . In this simulation, we assumed that the angle of the plane of incidence, ϕ , is given. In addition, we assumed that internal reflection would not occur.

5.3.3 Experimental Results of Object Rotation Method

Experiments using a hemispherical object

In order to determine the accuracy of the system, we use a plastic hemisphere having a refractive index of 1.5 and a diameter of 3cm.

Figure 5.7 illustrates the resultant shape of the hemisphere. Figure 5.7(a) represents the comparison between the theoretical shape and the obtained shape. Circle represents the theoretical shape and the plotted dots represent the obtained shape. Figure 5.7(b) represents the result 3D shape.

The height of the obtained shape seems to be lowered. The reason is that the obtained polarization degree is attenuated by internal reflection.

Because a transparent object reflects and transmits light, the observed intensity is the combination of the light reflected at the surface and the light transmitted from behind the object. We placed the object on a black pipe to block the light from behind the object. We should observe only the light reflected directly from the surface, but the shape of the object is not known a priori, so we cannot exactly estimate such internal reflection. We assume that any light which is not directly reflected from the surface

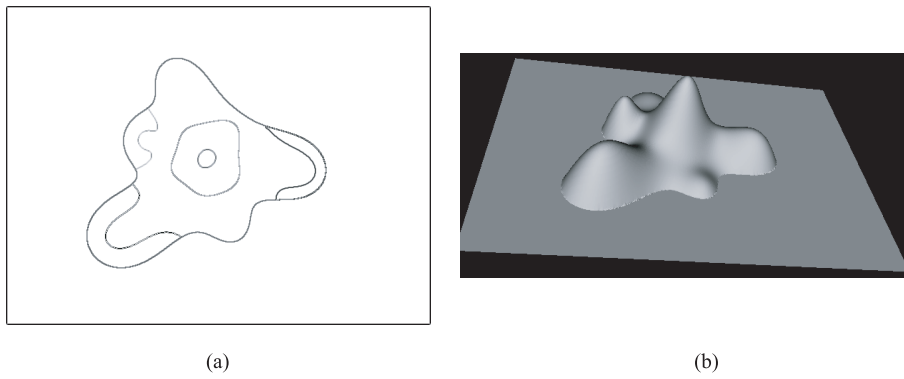


Figure 5.5: Simulation result of the object No.2. (a) Boundaries of each regions. (b) The result 3D-shape.

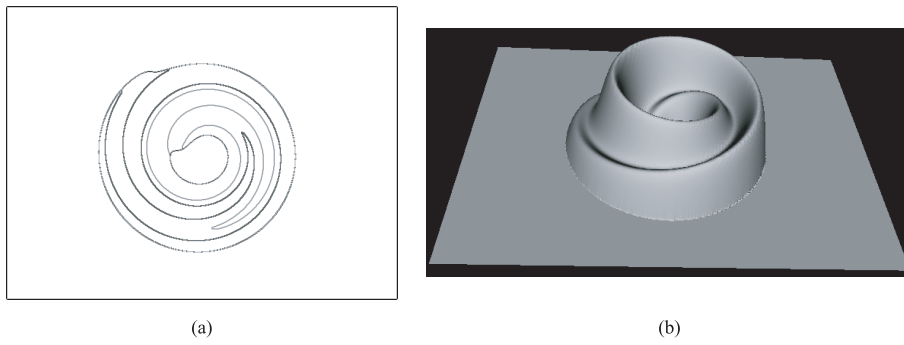


Figure 5.6: Simulation result of the object No.3. (a) Boundaries of each regions. (b) The result 3D-shape.

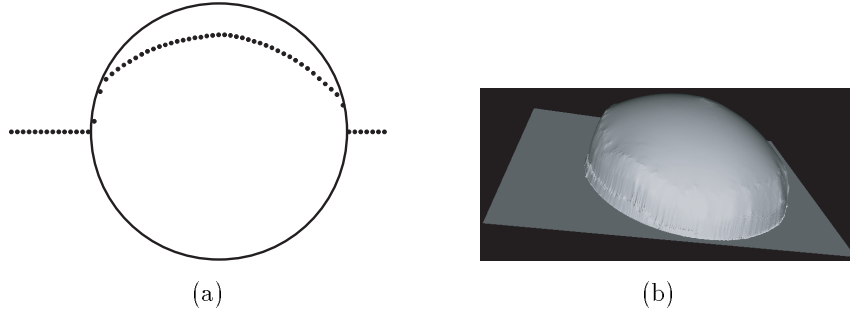


Figure 5.7: The result of the real hemisphere object. (a) Circle for the theoretical shape and the plotted dots for the obtained shape. (b) The result 3D-shape.

has an unpolarized, uniform intensity. Thus, we estimate the value of the intensity caused by the unintended reflection, and subtract the estimated value from all input images. This modification raises the maximum polarization degree of raw data to 1. A closed, continuous, and smooth object, which we assume, always has a Brewster angle, of which polarization degree equals to 1; thus, this modification is effective in any objects.

Figure 5.8 illustrates this modification effect. The theoretical value of the polarization degree is represented as a solid curve, and the obtained data is plotted as dots. Figure 5.8(a) is produced by using the raw data and Figure 5.8(b) is by modified data. At the range where the angle is bigger than the Brewster angle, the modified data is likely to fit the theoretically estimated value, while at the range where the angle is smaller than the Brewster angle, the modified polarization degree is still smaller than the theoretically estimated value. This result explains the reason for the height attenuation in Figure 5.7. In Figure 5.7, we can see that the angle bigger than the Brewster angle is likely to fit the theoretically estimated height, while the height where the angle is smaller than the Brewster angle is lower than the theoretically estimated height.

Table 5.1 shows the error of the hemisphere. Note that its diameter is 3cm. The error is an average error through all pixels. These errors are calculated as the difference between the true value and the experimental value.

Experiments using a bell-shaped object

In order to demonstrate the applicability of our system to an object of general shape, we determined the shape of the object shown in Figure 5.9(a). Figure 5.9(b) represents

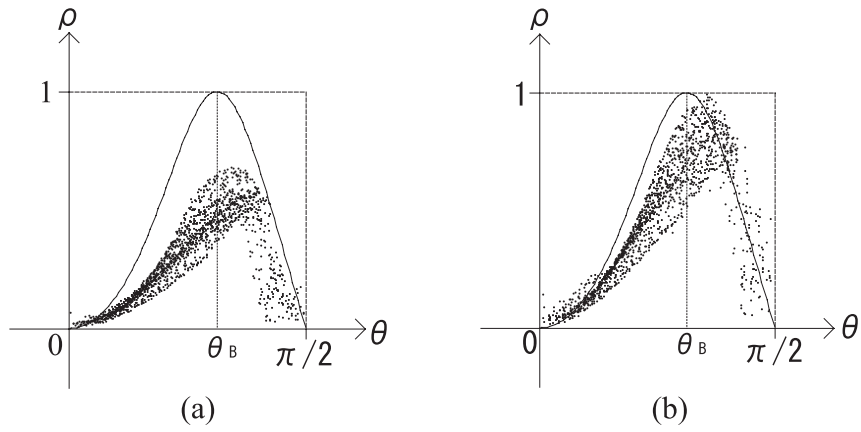


Figure 5.8: The graph of the polarization degree of the hemisphere object. (a) Raw data plotted. (b) Modified data plotted.

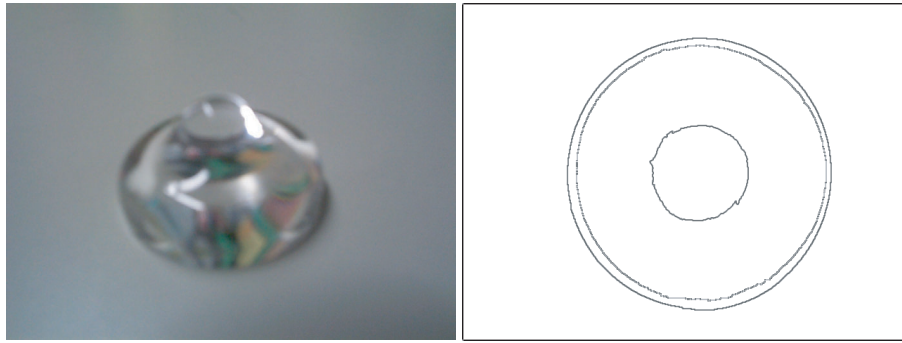
Polarization degree	0.173602
Angle of the incident plane, ϕ	20.573883°
Incident angle, θ	8.538068°
Surface normal	26.094410°
Height	2.649407mm

Table 5.1: Error of plastic transparent hemisphere

Brewster curves and occluding boundary. There are 3 regions. The bell-shaped object is made of acrylic and its refractive index is 1.5. We rotated the object approximately 8 degrees and obtained the data from two views. By applying our method to the obtained data, we finally obtain the distribution of the surface normal of the object. From this obtained distribution, a relaxation algorithm [26] converts the orientation distribution into a shape corresponding to that of the object. Figure 5.9(c) shows the obtained shape of the object, and Figure 5.9(d) shows an example of an rendering image of the object.

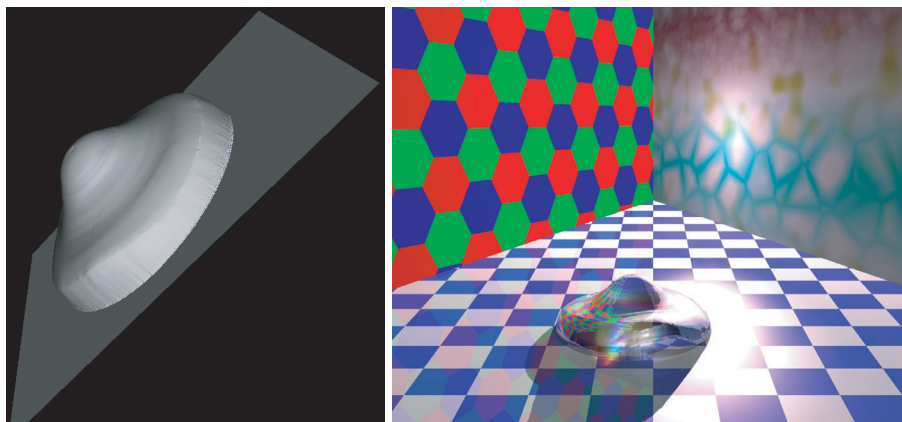
Figure 5.10 illustrates how the obtained shape fits the theoretical shape. Dots represent the obtained height data. A solid line represents the theoretical shape, which is obtained by hand using the edge of the photo of the object observed from the side of the object.

These figures prove that our method works relatively well; however, the obtained shape does not seem to be as precise as we would like it to be. The internal reflection of the object and the mutual reflection between the object and the experimental setup reduce the accuracy of the measurement.



(a)

(b)



(c)

(d)

Figure 5.9: The result for the bell-shaped real object. (a) A photo of the actual object. (b) Boundaries of each regions. (c) The result 3D-shape. (d) Rendering image of the object.

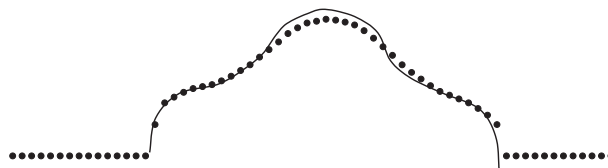


Figure 5.10: The result of the real bell-shaped object

Chapter 6

Conclusions

In this paper, we propose a method for determining the shape of a transparent object using polarization. Surface orientations are determined using the polarizations in visible light of a certain view. Because an algorithm using only one view in visible light provides ambiguities, polarization in infrared and polarization of the rotated object are then employed.

The thermal radiation, which also has characteristics of polarization, can be observed as infrared light. This polarization is an one-valued function; measuring polarization degree in infrared domain provides the emitting angle. However, the polarization degree is relatively low, and in some cases it is difficult to determine the polarization degree precisely. Thus, we propose to use polarization in both visible and infrared light.

By rotating the object, we also can disambiguate the angular problem. We obtain two set of data; one is for the object not rotated, and the other is for the object rotated in a small angle. We applied a Brewster segmentation to these data and divided into some regions. We calculated the difference of the polarization degree between these two set of data at the matching point, the point which surface normal lies along the rotation direction and which polarization degree is minimum in the B-B region. From that difference value, we determined the correct surface normal.

We have implemented the proposed method, and demonstrated its ability to determine the shape of a transparent object. First, we demonstrated the effectiveness of our proposed method through simulation. Second, by using a hemispherical object, we determined the accuracy of the method and demonstrated its effectiveness. Then, using an object of general shape, we demonstrated the ability of the system to determine the shapes of complex objects.

There are many beautiful glass objects of art in all over the world. However, those glass objects of art are hard but fragile. Those objects are always in danger of destruction. Many methods are proposed for modeling cultural heritages[27], though, there are few methods proposed for modeling glass objects of art. Our proposed method will be useful for modeling glass objects of art.

Our future work is to obtain the shape of transparent objects more accurately.

References

- [1] K. Ikeuchi, "Determining surface orientations of specular surfaces by using the photometric stereo method," *IEEE Trans. Patt. Anal. Mach. Intell.* **3**, 661-669 (1981).
- [2] S. K. Nayar, K. Ikeuchi, and T. Kanade, "Determining shape and reflectance of hybrid surface by photometric sampling," *IEEE Trans. Rob. Auto.* **6**, 418-431 (1990).
- [3] Y. Sato, M. D. Wheeler, and K. Ikeuchi, "Object shape and reflectance modeling from observation," in *Proc. SIGGRAPH 97*, (Addison Wesley, Boston, MA, 1997), pp.379-387.
- [4] M. Oren, and S. K. Nayar, "A theory of specular surface geometry," *International Journal of Computer Vision* **24** (2), 105-124 (1997).
- [5] K. Koshikawa, "A polarimetric approach to shape understanding of glossy objects," in *Proc. Int. Joint Conf. Artificial Intelligence*, (Morgan Kaufmann, Los Altos, CA, 1979), pp.493-495.
- [6] K. Koshikawa, and Y. Shirai, "A model-based recognition of glossy objects using their polarimetric properties," *Advanced Robotics* **2** (2), 137-147 (1987).
- [7] L. B. Wolff, "Polarization-based material classification from specular reflection," in *IEEE Trans. Patt. Anal. Mach. Intell.* **12** (11), 1059-1071 (1990).
- [8] L. B. Wolff and T. E. Boult, "Constraining object features using a polarization reflectance model," *IEEE Trans. Patt. Anal. Mach. Intell.* **13** (7), 635-657 (1991).
- [9] S. Rahmann and N. Canterakis, "Reconstruction of specular surfaces using polarization imaging," in *Proc. IEEE Conf. Computer Vision and Pattern Recognition*, (IEEE Computer Society Press, Los Alamitos, CA, 2001), pp.149-155.

- [10] D. L. Jordan and G. D. Lewis, "Measurements of the effect of surface roughness on the polarization state of thermally emitted radiation," *Opt. lett.*, **19**, 692-694, (1994).
- [11] D. L. Jordan, G. D. Lewis, and E. Jakeman, "Emission polarization of roughened glass and aluminum surfaces," *Appl. Opt.*, **35**, 3583-3590, (1996).
- [12] L. B. Wolff, A. Lundberg, and R. Tang, "Image understanding from thermal emission polarization," in *Proc. IEEE Conf. Computer Vision and Pattern Recognition*, (IEEE Computer Society Press, Los Alamitos, CA, 1998), pp.625-631.
- [13] R. Szeliski, S. Avidan, and P. Anandan, "Layer extraction from multiple images containing reflections and transparency," in *Proc. IEEE Conf. Computer Vision and Pattern Recognition*, (IEEE Computer Society Press, Los Alamitos, CA, 2000), pp.246-253.
- [14] Y. Schechner, J. Shamir, and N. Kiryuati, "Polarization-based decorrelation of transparent layers: the inclination angle of an invisible surface," in *Proc. IEEE Int. Conf. Computer Vision*, (IEEE Computer Society Press, Los Alamitos, CA, 1999), pp.814-819.
- [15] D. E. Zongker, D. M. Warner, B. Curless, and D. H. Salesin, "Environmental matting and compositing," in *Proc. SIGGRAPH 99*, (Addison Wesley, Boston, MA, 1999), pp.205-214.
- [16] Y. Chuang, D. E. Zongker, J. Hindorff, B. Curless, D. H. Salesin, and R. Szeliski, "Environment matting extensions: towards higher accuracy and real-time capture," in *Proc. SIGGRAPH 2000*, (Addison Wesley, Boston, MA, 2000), pp.121-130.
- [17] M. Saito, Y. Sato, K. Ikeuchi, and H. Kashiwagi, "Measurement of surface orientations of transparent objects using polarization in highlight," in *Proc. IEEE Conf. Computer Vision and Pattern Recognition*, (IEEE Computer Society Press, Los Alamitos, CA, 1999), pp.381-386.
- [18] M. Saito, Y. Sato, K. Ikeuchi, and H. Kashiwagi, "Measurement of surface orientations of transparent objects by use of polarization in highlight," *J. Opt Soc. Am. A* **16** (9), 2286-2293 (1999).
- [19] K. E. Torrance and E. M. Sparrow, "Theory for off-specular reflection from roughened surfaces," *J. Opt. Soc. Am.* **57** (9), 1105-1114 (1967).

- [20] M. Born, and E. Wolf, *Principles of optics*, (Pergamon, New York, 1959).
- [21] F. E. Nicodemus, "Directional reflectance and emissivity of an opaque surface," *Appl. Opt.*, **4**, 767-773, (1965).
- [22] F. E. Nicodemus, "Reflectance nomenclature and directional reflectance and emissivity," *Appl. Opt.*, **9**, 1474-1475, (1970).
- [23] O. Sandus, "A review of emission polarization," *Appl. Opt.*, **4** (12), 1634-1642 (1965).
- [24] M. P. do Carmo, *Differential geometry of curves and surfaces*, (Prentice-Hall, New Jersey, 1976).
- [25] B. K. P. Horn, *Robot vision*, (Mit Press, Cambridge, 1986).
- [26] K. Ikeuchi, "Reconstructing a depth map from intensity maps," in *Proc. Int. Conf. on Pattern Recognition*, (IEEE Computer Society Press, Los Alamitos, CA, 1984), pp.736-738.
- [27] D. Miyazaki, T. Oishi, T. Nishikawa, R. Sagawa, K. Nishino, T. Tomomatsu, Y. Takase, and K. Ikeuchi, "The Great Buddha Project: Modeling Cultural Heritage through Observation," in *Proc. Int. Conf. Virtual Systems and MultiMedia*, (2000), pp.138-145.
- [28] S. K. Nayar, K. Ikeuchi, T. Kanade, "Surface reflection: Physical and geometrical perspectives," *IEEE Trans. Patt. Anal. Mach. Intell.*, **13**, 611, (1991).
- [29] S. Shafer, "Using color to separate reflection components," *COLOR Research and Application*, **10**, 210, (1985).
- [30] L. B. Wolff, "Spectral and polarization stereo methods using a single light source," *Proceedings of ICCV*, 708, (1987).
- [31] S. K. Nayar, X. S. Fang, and T. Boult, "Separation of reflection components using color and polarization," *Int. J. Com. Vision*, **21**, 163, (1997).
- [32] D. Miyazaki, M. Saito, Y. Sato, K. Ikeuchi, "Shape Measurement of Transparent Objects using Polarization and Geometrical Characteristics," *IPSJ Transactions on Computer Vision and Image Media 2000-CVIM-123* pp.33-42, September, 2000.

- [33] K. Ikeuchi, Y. Takase, T. Tomomatsu, K. Nishino, R. Sagawa, T. Nishikawa, T. Oishi, D. Miyazaki, "Applying MFR(modelling-from-reality) for Cultural Heritage Preservation," Korea-Japan Joint Workshop on Network Based Human Friendly Mechatronics and Systems, pp.66-70, November, 2000.
- [34] K. Ikeuchi, Y. Takase, K. Nishino, R. Sagawa, D. Miyazaki, T. Oishi, "Modelling Cultural Heritage through Observation," 7th International Display Workshop, pp.1099-1102, November, 2000.
- [35] K. Ikeuchi, Y. Sato, K. Nishino, R. Sagawa, T. Nishikawa, T. Oishi, I. Sato, J. Takamatsu and D. Miyazaki, "Modeling Cultural Heritage through Observation", in Proc. of IEEE First Pacific-Rim Conference on Multimedia, Dec., 2000

Appendix A

Theory of Optics (In More Detail)

A.1 Maxwell's equations

Maxwell's equations for arbitrary mediums are,

$$\begin{aligned}\operatorname{rot}\mathbf{E} &= -\frac{\partial\mathbf{B}}{\partial t} \\ \operatorname{rot}\mathbf{H} &= \mathbf{j} + \frac{\partial\mathbf{D}}{\partial t} \\ \operatorname{div}\mathbf{D} &= \rho \\ \operatorname{div}\mathbf{B} &= 0\end{aligned}$$

, where \mathbf{E} is electric vector, \mathbf{B} is magnetic induction, t is time, \mathbf{H} is magnetic vector, \mathbf{j} is electric current density, \mathbf{D} is electric displacement, ρ is charge density. These equations represents,

1. Faraday's electromagnetic induction law
2. Ampère's law
3. Gauss' law
4. magnetic monopole does not exist

, respectively. Following equations relates \mathbf{E} to \mathbf{D} and \mathbf{H} to \mathbf{B} respectively.

$$\begin{aligned}\mathbf{D} &= \varepsilon_0\mathbf{E} + \mathbf{P} \\ \mathbf{B} &= \mu_0(\mathbf{H} + \mathbf{M})\end{aligned}$$

, where \mathbf{P} is electrolytic polarization, \mathbf{M} is magnetization, ε_0 is dielectric permittivity of vacuum, μ_0 is magnetic permeability of vacuum.

Dielectric (*or* insulator) medium does not include electric charge, and does not produce electric current when electric field appears. For isotropic dielectrics, following equations hold.

$$\rho = 0$$

$$\mathbf{j} = 0$$

$$\mathbf{D} = \varepsilon \mathbf{E}$$

$$\mathbf{B} = \mu \mathbf{H}$$

Thus, Maxwell's equations for isotropic dielectrics (include vacuum) will be,

$$\text{rot} \mathbf{E} = -\mu \frac{\partial \mathbf{H}}{\partial t} \quad (\text{A.1})$$

$$\text{rot} \mathbf{H} = \varepsilon \frac{\partial \mathbf{E}}{\partial t} \quad (\text{A.2})$$

$$\text{div} \mathbf{E} = 0 \quad (\text{A.3})$$

$$\text{div} \mathbf{H} = 0 \quad (\text{A.4})$$

, where ε is dielectric permittivity, and μ is magnetic permeability.

Following equations are defined in the research field of vector analysis.

$$\nabla \mathbf{A} = \text{grad} \mathbf{A} = \begin{pmatrix} \frac{\partial A_x}{\partial x} \\ \frac{\partial A_y}{\partial y} \\ \frac{\partial A_z}{\partial z} \end{pmatrix}$$

$$\nabla \times \mathbf{A} = \text{rot} \mathbf{A} = \text{curl} \mathbf{A} = \begin{pmatrix} \frac{\partial A_z}{\partial y} - \frac{\partial A_y}{\partial z} \\ \frac{\partial A_x}{\partial z} - \frac{\partial A_z}{\partial x} \\ \frac{\partial A_y}{\partial x} - \frac{\partial A_x}{\partial y} \end{pmatrix}$$

$$\nabla \cdot \mathbf{A} = \text{div} \mathbf{A} = \frac{\partial A_x}{\partial x} + \frac{\partial A_y}{\partial y} + \frac{\partial A_z}{\partial z}$$

$$\nabla^2 \mathbf{A} = \Delta \mathbf{A} = \frac{\partial^2 A_x}{\partial x^2} + \frac{\partial^2 A_y}{\partial y^2} + \frac{\partial^2 A_z}{\partial z^2}$$

, where

$$\mathbf{A} = \begin{pmatrix} A_x \\ A_y \\ A_z \end{pmatrix}$$

From above equations, the following equation can be derived.

$$\text{rot rot} = \text{grad div} - \nabla^2 \quad (\text{A.5})$$

By calculating $\partial/\partial t$ of both sides of Equation (A.1), we obtain the following equation by using Equations (A.2), (A.4) and (A.5).

$$\begin{aligned}
-\mu \frac{\partial^2 \mathbf{H}}{\partial t^2} &= \frac{\partial}{\partial t}(\text{rot} \mathbf{E}) \\
&= \text{rot} \frac{\partial \mathbf{E}}{\partial t} \\
&= \frac{1}{\varepsilon} \text{rot}(\text{rot} \mathbf{H}) \\
&= \frac{1}{\varepsilon} (\text{grad}(\text{div} \mathbf{H}) - \nabla^2 \mathbf{H}) \\
&= -\frac{1}{\varepsilon} \nabla^2 \mathbf{H}
\end{aligned}$$

Thus,

$$\nabla^2 \mathbf{H} = \varepsilon \mu \frac{\partial^2 \mathbf{H}}{\partial t^2}$$

Similarly,

$$\nabla^2 \mathbf{E} = \varepsilon \mu \frac{\partial^2 \mathbf{E}}{\partial t^2}$$

These equations are wave equation which is ordinarily expressed as,

$$\nabla^2 \mathbf{A} = \frac{1}{v^2} \frac{\partial^2 \mathbf{A}}{\partial t^2}$$

, where v is the propagating speed of the wave. Thus, the speed of electromagnetic wave will be,

$$v = \frac{1}{\sqrt{\varepsilon \mu}}$$

By denoting ε_0 as the ε in vacuum and μ_0 as the μ in vacuum, the light speed c in vacuum can be expressed as,

$$c = \frac{1}{\sqrt{\varepsilon_0 \mu_0}}$$

In almost all mediums except for magnetic mediums, $\mu = \mu_0$ holds. The ratio of the light speed in vacuum to that in the medium is called refractive index of the medium.

$$n = \frac{c}{v} = \sqrt{\frac{\varepsilon}{\varepsilon_0}} \tag{A.6}$$

A.2 Electric Field and Magnetic Field

Plane wave is expressed as,

$$\mathbf{A} \exp\{-i(\omega t - \mathbf{k} \cdot \mathbf{r})\}$$

, where \mathbf{A} is amplitude, i is an imaginary number, ω is angular frequency, t is time, \mathbf{k} is wave vector (*or* propagation vector), \mathbf{r} is position vector. From the definition of wave, $\omega = 2\pi\nu$, $v = \lambda\nu$ and $\lambda_0 = n\lambda$, where ν is frequency, λ is wavelength, λ_0 is that in vacuum and n is refractive index. Wave vector is defined as $\mathbf{k} = k\mathbf{n}$, where k is wave number and \mathbf{n} is the unit vector which represents the direction of the propagation of the wave.

$$k = \frac{\omega}{v} = \frac{2\pi}{\lambda} = \frac{2\pi n}{\lambda_0} = \omega\sqrt{\varepsilon\mu_0} \quad (\text{A.7})$$

From,

$$\mathbf{k} = \begin{pmatrix} k_x \\ k_y \\ k_z \end{pmatrix}, \quad \mathbf{n} = \begin{pmatrix} x \\ y \\ z \end{pmatrix}$$

, we can derive,

$$\frac{\partial \mathbf{k} \cdot \mathbf{r}}{\partial x} = k_x, \quad \frac{\partial \mathbf{k} \cdot \mathbf{r}}{\partial y} = k_y, \quad \frac{\partial \mathbf{k} \cdot \mathbf{r}}{\partial z} = k_z$$

The electric field and the magnetic field of plane wave is expressed as,

$$\begin{aligned} \mathbf{E} &= \mathbf{E}_0 \exp\{-i(\omega t - \mathbf{k} \cdot \mathbf{r})\} \\ \mathbf{H} &= \mathbf{H}_0 \exp\{-i(\omega t - \mathbf{k} \cdot \mathbf{r})\} \end{aligned}$$

, where \mathbf{E}_0 and \mathbf{H}_0 are constant complex vector. By calculating $\partial/\partial t$ of \mathbf{E} and \mathbf{H} , we obtain,

$$\frac{\partial \mathbf{E}}{\partial t} = -i\omega \mathbf{E} \quad (\text{A.8})$$

$$\frac{\partial \mathbf{H}}{\partial t} = -i\omega \mathbf{H} \quad (\text{A.9})$$

We denote the x -component of $\text{rot}\mathbf{E}$ as $(\text{rot}\mathbf{E})_x$ and we obtain,

$$\begin{aligned} (\text{rot}\mathbf{E})_x &= \frac{\partial E_z}{\partial y} - \frac{\partial E_y}{\partial z} \\ &= i(k_y E_z - k_z E_y) \\ &= i(\mathbf{k} \times \mathbf{E})_x \end{aligned}$$

Similarly we obtain,

$$(\text{rot}\mathbf{E})_y = i(\mathbf{k} \times \mathbf{E})_y, \quad (\text{rot}\mathbf{E})_z = i(\mathbf{k} \times \mathbf{E})_z$$

Thus,

$$\text{rot}\mathbf{E} = i\mathbf{k} \times \mathbf{E} \quad (\text{A.10})$$

By applying the above derivation to \mathbf{H} , we also obtain,

$$\text{rot}\mathbf{H} = i\mathbf{k} \times \mathbf{H} \quad (\text{A.11})$$

By substituting Equation (A.10) and (A.9) into Equation (A.1), we obtain,

$$\mathbf{k} \times \mathbf{E} = \omega\mu\mathbf{H} \quad (\text{A.12})$$

By substituting Equation (A.11) and (A.8) into Equation (A.2), we obtain,

$$\mathbf{k} \times \mathbf{H} = -\omega\varepsilon\mathbf{E} \quad (\text{A.13})$$

By calculating the dot product of \mathbf{k} with Equations (A.12), (A.13), we obtain,

$$\begin{aligned} \mathbf{E} \cdot \mathbf{k} &= -\frac{1}{\omega\varepsilon}(\mathbf{k} \times \mathbf{H}) \cdot \mathbf{k} = 0 \\ \mathbf{H} \cdot \mathbf{k} &= \frac{1}{\omega\mu}(\mathbf{k} \times \mathbf{E}) \cdot \mathbf{k} = 0 \end{aligned}$$

These equations indicates that the oscillation of the electric field \mathbf{E} and the magnetic field \mathbf{H} is orthogonal to the propagation direction \mathbf{k} , concluding that light is a transversal wave. From Equation (A.12) or (A.13), we obtain,

$$\mathbf{E} \cdot \mathbf{H} = -\frac{1}{\omega\varepsilon}\mathbf{H} \cdot (\mathbf{k} \times \mathbf{H}) = \frac{1}{\omega\mu}\mathbf{E} \cdot (\mathbf{k} \times \mathbf{E}) = 0$$

Thus, \mathbf{E} and \mathbf{H} is also orthogonal. By calculating the absolute value of both sides of Equation (A.12) or (A.13) using Equation (A.7), we obtain,

$$\sqrt{\varepsilon}|\mathbf{E}| = \sqrt{\mu_0}|\mathbf{H}| \quad (\text{A.14})$$

A.3 Poynting Vector and Intensity

Poynting vector is defined as,

$$\mathbf{S} = \mathbf{E} \times \mathbf{H}$$

This represents the propagation direction and the instantaneous energy density per unit time and per unit area, propagates by the electromagnetic field. We call the light energy per unit time and per unit area as intensity and represent as I . I is expressed as $I = \langle |\mathbf{S}| \rangle$, where $\langle \rangle$ represents the time average.

$$\begin{aligned} I &= \langle |\mathbf{S}| \rangle \\ &= \frac{1}{2}|\mathbf{E}||\mathbf{H}| \\ &= \frac{1}{2}\sqrt{\frac{\varepsilon}{\mu_0}}|\mathbf{E}|^2 \\ &= \frac{n}{2}\sqrt{\frac{\varepsilon_0}{\mu_0}}|\mathbf{E}|^2 \end{aligned} \quad (\text{A.15})$$

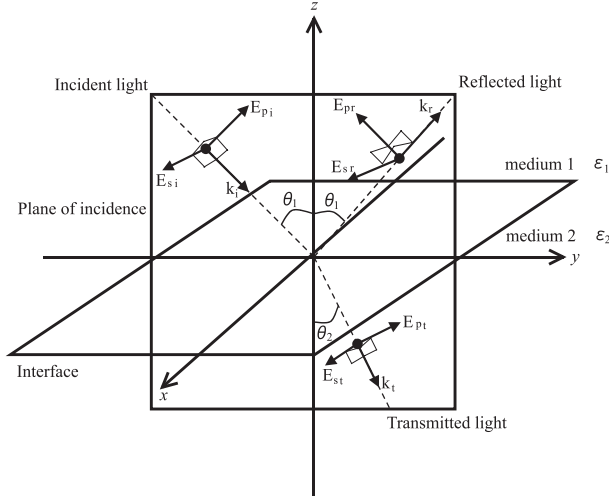


Figure A.1: Electric vector

A.4 Fresnel formulae

Consider the interface of medium 1 (dielectric permittivity ε_1) and medium 2 (dielectric permittivity ε_2) lies in the xy -plane and the plane of incidence lies in the yz -plane (Figure A.1 and Figure A.2). (Note: This definition is different from Figure 2.1.) We denote the incident angle, the reflected angle, the transmitted angle, as θ_1 , θ_1 , θ_2 , respectively. The electric amplitude of the incident light, the reflected light, the transmitted light is denoted as \mathbf{E}_{0i} , \mathbf{E}_{0r} , \mathbf{E}_{0t} , respectively, and the magnetic amplitude of those are denoted as \mathbf{H}_{0i} , \mathbf{H}_{0r} , \mathbf{H}_{0t} , respectively. We divide these lights in p -component, which is parallel to the plane of incidence, and s -component, which is parallel to x -axis. Then the light can be expressed as the following vectors.

$$\mathbf{E}_{0i} = \begin{pmatrix} E_s^i \\ E_p^i \cos \theta_1 \\ E_p^i \sin \theta_1 \end{pmatrix}, \quad \mathbf{E}_{0r} = \begin{pmatrix} E_s^r \\ -E_p^r \cos \theta_1 \\ E_p^r \sin \theta_1 \end{pmatrix}, \quad \mathbf{E}_{0t} = \begin{pmatrix} E_s^t \\ E_p^t \cos \theta_2 \\ E_p^t \sin \theta_2 \end{pmatrix}$$

$$\mathbf{H}_{0i} = \begin{pmatrix} H_p^i \\ -H_s^i \cos \theta_1 \\ -H_s^i \sin \theta_1 \end{pmatrix}, \quad \mathbf{H}_{0r} = \begin{pmatrix} H_p^r \\ H_s^r \cos \theta_1 \\ -H_s^r \sin \theta_1 \end{pmatrix}, \quad \mathbf{H}_{0t} = \begin{pmatrix} H_p^t \\ -H_s^t \cos \theta_2 \\ -H_s^t \sin \theta_2 \end{pmatrix}$$

At the interface $z = 0$, because of the continuity of the light wave, the sum of the amplitude of the incident light and the reflected light, which both are in the medium 1, must be equal to the amplitude of the transmitted light, which is in the medium 2,

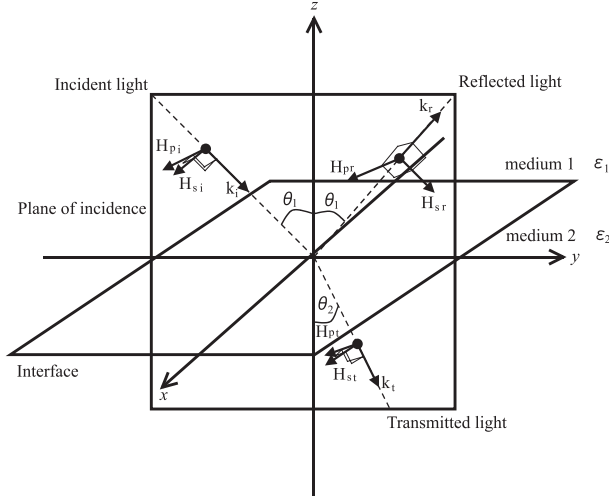


Figure A.2: Magnetic vector

for each x -component and y -component. Thus, the following equations hold.

$$\begin{aligned}
 E_s^i + E_s^r &= E_s^t \\
 E_p^i \cos \theta_1 - E_p^r \cos \theta_1 &= E_p^t \cos \theta_2 \\
 H_p^i + H_p^r &= H_p^t \\
 H_s^i \cos \theta_1 - H_s^r \cos \theta_1 &= H_s^t \cos \theta_2
 \end{aligned}$$

By substituting $H = \sqrt{\varepsilon/\mu_0}E$ and Snell's law $\sqrt{\varepsilon_1} \sin \theta_1 = \sqrt{\varepsilon_2} \sin \theta_2$, the above equations can be rewritten as,

$$E_s^i + E_s^r = E_s^t \quad (\text{A.16})$$

$$(E_p^i - E_p^r) \cos \theta_1 = E_p^t \cos \theta_2 \quad (\text{A.17})$$

$$(E_p^i + E_p^r) \sin \theta_2 = E_p^t \sin \theta_1 \quad (\text{A.18})$$

$$(E_s^i - E_s^r) \tan \theta_2 = E_s^t \tan \theta_1 \quad (\text{A.19})$$

The ratio of the amplitude of the reflected light to that of the incident light is called amplitude reflectivity, and the ratio of the amplitude of the transmitted light to that of the incident light is called amplitude transmissivity. The amplitude reflectivity r and the amplitude transmissivity t of p -component and s -component is defined as,

$$r_p = \frac{E_p^r}{E_p^i}, \quad r_s = \frac{E_s^r}{E_s^i}, \quad t_p = \frac{E_p^t}{E_p^i}, \quad t_s = \frac{E_s^t}{E_s^i}$$

From Equation (A.17) and (A.18),

$$E_p^t = (E_p^i - E_p^r) \frac{\cos \theta_1}{\cos \theta_2} = (E_p^i + E_p^r) \frac{\sin \theta_2}{\sin \theta_1}$$

i.e. $(1 - r_p) \sin \theta_1 \cos \theta_1 = (1 + r_p) \sin \theta_2 \cos \theta_2$

Thus,

$$\begin{aligned} r_p &= \frac{\sin \theta_1 \cos \theta_1 - \sin \theta_2 \cos \theta_2}{\sin \theta_1 \cos \theta_1 + \sin \theta_2 \cos \theta_2} \\ &= \frac{\sin 2\theta_1 - \sin 2\theta_2}{\sin 2\theta_1 + \sin 2\theta_2} \\ &= \frac{\cos(\theta_1 + \theta_2) \sin(\theta_1 - \theta_2)}{\sin(\theta_1 + \theta_2) \cos(\theta_1 - \theta_2)} \\ &= \frac{\tan(\theta_1 - \theta_2)}{\tan(\theta_1 + \theta_2)} \end{aligned} \tag{A.20}$$

From Equation (A.16) and (A.19),

$$E_s^t = E_s^i + E_s^r = (E_s^i - E_s^r) \frac{\tan \theta_2}{\tan \theta_1}$$

i.e. $(1 + r_s) \tan \theta_1 = (1 - r_s) \tan \theta_2$

Thus,

$$\begin{aligned} r_s &= -\frac{\tan \theta_1 - \tan \theta_2}{\tan \theta_1 + \tan \theta_2} \\ &= -\frac{\sin \theta_1 \cos \theta_2 - \cos \theta_1 \sin \theta_2}{\sin \theta_1 \cos \theta_2 + \cos \theta_1 \sin \theta_2} \\ &= -\frac{\sin(\theta_1 + \theta_2) + \sin(\theta_1 - \theta_2) - \sin(\theta_1 + \theta_2) + \sin(\theta_1 - \theta_2)}{\sin(\theta_1 + \theta_2) + \sin(\theta_1 - \theta_2) + \sin(\theta_1 + \theta_2) - \sin(\theta_1 - \theta_2)} \\ &= -\frac{\sin(\theta_1 - \theta_2)}{\sin(\theta_1 + \theta_2)} \end{aligned} \tag{A.21}$$

From Equation (A.17) and (A.18),

$$E_p^r = E_p^i - E_p^t \frac{\cos \theta_2}{\cos \theta_1} = -E_p^i + E_p^t \frac{\sin \theta_1}{\sin \theta_2}$$

i.e. $\cos \theta_1 \sin \theta_2 - t_p \cos \theta_2 \sin \theta_2 = -\sin \theta_2 \cos \theta_1 + t_p \sin \theta_1 \cos \theta_1$

Thus,

$$\begin{aligned} t_p &= \frac{2 \sin \theta_2 \cos \theta_1}{\sin \theta_1 \cos \theta_1 + \sin \theta_2 \cos \theta_2} \\ &= \frac{2 \sin \theta_2 \cos \theta_1}{\frac{1}{2} \sin 2\theta_1 + \frac{1}{2} \sin 2\theta_2} \\ &= \frac{2 \sin \theta_2 \cos \theta_1}{\sin(\theta_1 + \theta_2) \cos(\theta_1 - \theta_2)} \end{aligned} \tag{A.22}$$

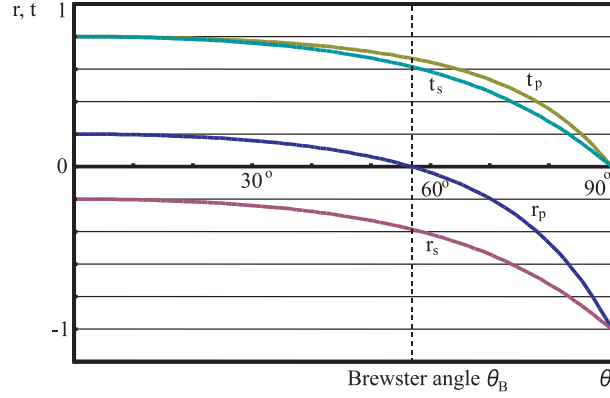


Figure A.3: Amplitude reflectivity and amplitude transmissivity

From Equation (A.16) and (A.19),

$$E_s^r = E_s^t - E_s^i = E_s^i - E_s^t \frac{\tan \theta_1}{\tan \theta_2}$$

i.e. $(t_s - 1) \tan \theta_2 = \tan \theta_2 - t_s \tan \theta_1$

Thus,

$$\begin{aligned} t_s &= \frac{2 \tan \theta_2}{\tan \theta_1 + \tan \theta_2} \\ &= \frac{2 \sin \theta_2 \cos \theta_1}{\sin \theta_1 \cos \theta_2 + \cos \theta_1 \sin \theta_2} \\ &= \frac{2 \sin \theta_2 \cos \theta_1}{\frac{1}{2} \sin(\theta_1 + \theta_2) + \frac{1}{2} \sin(\theta_1 - \theta_2) + \frac{1}{2} \sin(\theta_1 + \theta_2) - \frac{1}{2} \sin(\theta_1 - \theta_2)} \\ &= \frac{2 \sin \theta_2 \cos \theta_1}{\sin(\theta_1 + \theta_2)} \end{aligned} \quad (\text{A.23})$$

Equations (A.20), (A.21), (A.22), (A.23) are called Fresnel's law (Figure A.3).

A.5 Derivation of Intensity Ratio

The light energy at the interface per unit area is expressed by using Equation (A.15) as,

$$\begin{aligned} \text{Incident Light } I_i &= \frac{n_1}{2} \sqrt{\frac{\varepsilon_0}{\mu_0}} E_{0i}^2 \cos \theta_1 \\ \text{Reflected Light } I_r &= \frac{n_1}{2} \sqrt{\frac{\varepsilon_0}{\mu_0}} E_{0r}^2 \cos \theta_1 \end{aligned}$$

$$\text{Transmitted Light } I_t = \frac{n_2}{2} \sqrt{\frac{\varepsilon_0}{\mu_0}} E_{0t}^2 \cos \theta_2$$

The intensity reflectivity of p -component F_p and that of s -component F_s are,

$$F_p = \left(\frac{I_r}{I_i} \right)_p = \left(\frac{E_{0r}}{E_{0i}} \right)_p^2 = r_p^2$$

$$F_s = \left(\frac{I_r}{I_i} \right)_s = \left(\frac{E_{0r}}{E_{0i}} \right)_s^2 = r_s^2$$

From this equations and Equation (A.20) and (A.21), we can derive Equation (2.1).

The intensity transmissivity of p -component T_p and that of s -component T_s are,

$$T_p = \left(\frac{I_t}{I_i} \right)_p = \left(\frac{E_{0t}}{E_{0i}} \right)_p^2 \frac{n_2 \cos \theta_2}{n_1 \cos \theta_1} = \frac{n_2 \cos \theta_2}{n_1 \cos \theta_1} t_p^2$$

$$T_s = \left(\frac{I_t}{I_i} \right)_s = \left(\frac{E_{0t}}{E_{0i}} \right)_s^2 \frac{n_2 \cos \theta_2}{n_1 \cos \theta_1} = \frac{n_2 \cos \theta_2}{n_1 \cos \theta_1} t_s^2$$

From this equations and Equation (A.22) and (A.23) and Snell's law $n_1 \sin \theta_1 = n_2 \sin \theta_2$, we can derive Equation (3.4).

A.6 Graph of Intensity Ratio

By substituting Snell's law into Equation (2.1), we obtain,

$$F_p = \frac{1 + n^2 - (n^2 + 1/n^2) \sin^2 \theta - 2 \cos \theta \sqrt{n^2 - \sin^2 \theta}}{1 + n^2 - (n^2 + 1/n^2) \sin^2 \theta + 2 \cos \theta \sqrt{n^2 - \sin^2 \theta}}$$

$$F_s = \frac{1 + n^2 - 2 \sin^2 \theta - 2 \cos \theta \sqrt{n^2 - \sin^2 \theta}}{1 + n^2 - 2 \sin^2 \theta + 2 \cos \theta \sqrt{n^2 - \sin^2 \theta}}$$

By substituting Snell's law into Equation (3.4), we obtain,

$$T_p = \frac{4 \cos \theta \sqrt{n^2 - \sin^2 \theta}}{1 + n^2 - (n^2 + 1/n^2) \sin^2 \theta + 2 \cos \theta \sqrt{n^2 - \sin^2 \theta}}$$

$$T_s = \frac{4 \cos \theta \sqrt{n^2 - \sin^2 \theta}}{1 + n^2 - 2 \sin^2 \theta + 2 \cos \theta \sqrt{n^2 - \sin^2 \theta}}$$

These graph are depicted in Figure A.4. The graphs with the tags written as F_p and F_s are the graphs of the parallel and perpendicular intensity ratios of reflection, respectively. The graphs with the tags written as T_p and T_s are the graphs of the parallel and perpendicular intensity ratios of transmission, respectively.

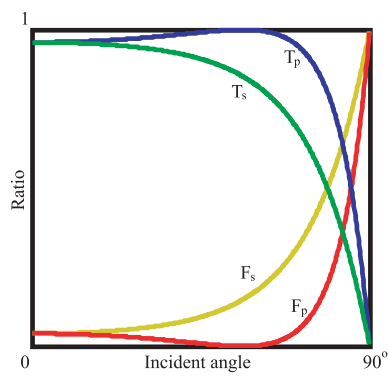


Figure A.4: Graphs of intensity ratios

Appendix B

Gaussian Mapping

Consider translating the starting point of the unit surface normal vector \mathbf{n}_P at the point P of the surface S to the origin of the coordinate axes. Therefore, the end of the unit surface normal vector lies on an unit sphere and let us denote this point as $g(P)$. We call the mapping,

$$g : S \longrightarrow \text{unit sphere} \tag{B.1}$$

as Gaussian mapping. Figure B.1 depicts a Gaussian mapping.

We will explain in more detail (Figure B.2).

The Gaussian mapping of a sphere whose radius is R is depicted in Figure B.2(a). The point P and Q of the sphere maps onto the point $g(P)$ and $g(Q)$, respectively, on unit sphere, where each surface normal is the same. Scaling the sphere of radius R to an unit sphere will be the Gaussian mapping, namely, the similarity mapping of similarity ratio $1/R$ will be the Gaussian mapping.

The Gaussian mapping of a kind of a lemon is depicted in Figure B.2(b). The upper part of the lemon is scale-downed by Gaussian mapping near to the north pole of the unit sphere, while, the sharp part of the lemon extends by Gaussian mapping to almost an half of the unit sphere. You will see that the degree of curving surfaces is in proportion to the scale of the mapped part of the unit sphere to the surface part.

How the elliptic surface maps onto the unit sphere by Gaussian mapping was shown in Figure B.2(b), whereas, how the hyperbolic surface maps onto the unit sphere by Gaussian mapping is shown in Figure B.2(c). The left and the right part around P maps inversely to the right and the left part around $g(P)$. The small area around P reversely maps to the small area around $g(P)$. You will see that hyperbolic surface reversely maps onto the unit sphere by Gaussian mapping.

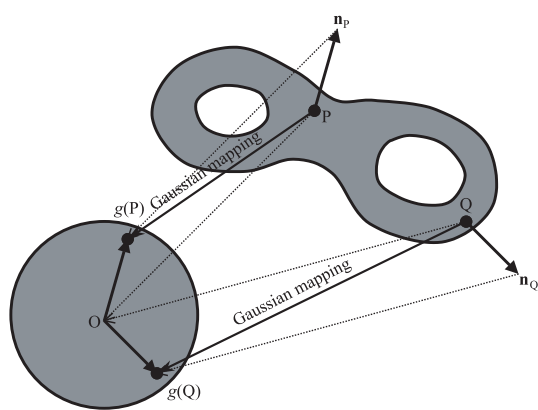


Figure B.1: Gaussian mapping

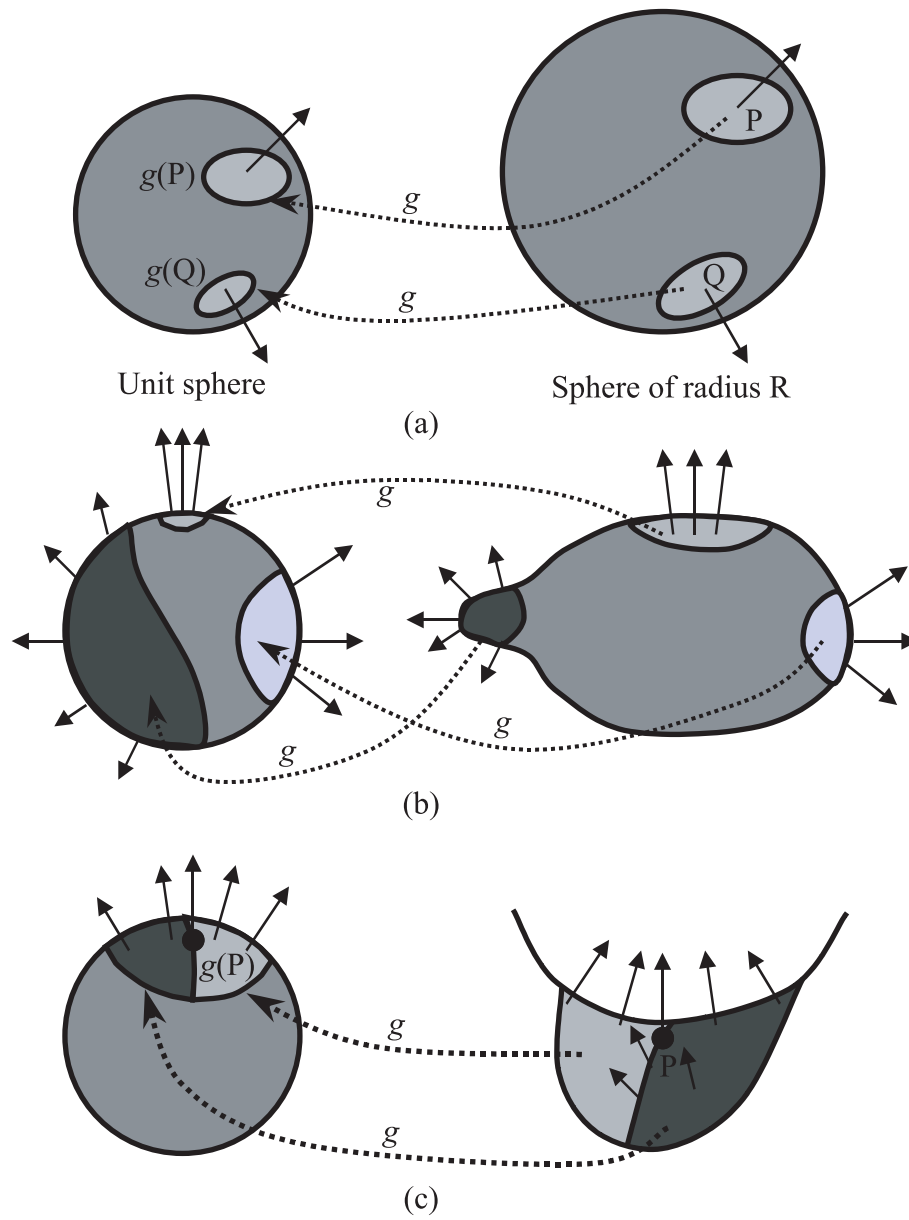


Figure B.2: Three examples of Gaussian mapping

Appendix C

Fitting Sine Curve

By rotating a polarization filter, we obtain a sequence of images of an object. We measure from 0 degrees through 175 degrees at 5 degree intervals. From this process we obtain 36 images.

At each pixel of the 36 images, we observe variance of intensity and determine the maximum and minimum intensities, I_{\max} and I_{\min} . Because those measurements occur at 5 degree intervals, it is difficult to obtain the exact maximum and minimum values. By using the least square minimization, we fit a sinusoidal curve to those obtained measurements, then determine the maximum and minimum values. The sinusoidal function we used has three parameters. Although general sinusoidal function requires four parameters, the fact that the polarization filter has a cycle of 180 degrees through rotation reduces the required number of parameters to three. Thus, the sinusoidal function which we want to fit can be expressed as;

$$y = A \sin 2(x - B) + C \quad [A > 0, -\pi < B < 0] . \quad (\text{C.1})$$

Fitting this sinusoidal curve by the least square minimization is a non-linear fitting and is difficult to manage (, though it can be calculated by using Levenberg-Marquardt method, etc). Thus, we first fit the linear sinusoidal curve, which is expressed as;

$$y = a \sin 2x + b \cos 2x + C \quad (\text{C.2})$$

, by the linear least square minimization and transformed this equation into Equation (C.1). From $I_{\max} = C + A$ and $I_{\min} = C - A$ (and two ϕ s by $\phi = B + \frac{3}{4}\pi + n\pi$ [$0 \leq \phi < 2\pi$]), we determine two possible incident angles using Equation (2.4) and (2.5).

Equations (C.1) and (C.2) are related by the following formulae.

$$a \sin \theta + b \cos \theta = \sqrt{a^2 + b^2} \sin(\theta + \alpha)$$

$$\sin \alpha = \frac{b}{\sqrt{a^2 + b^2}}$$

$$\cos \alpha = \frac{a}{\sqrt{a^2 + b^2}}$$

Appendix D

Relaxation Method

We calculate the surface shape from surface normal using relaxation method. The acquired surface normal have some errors in the value, so we must use an appropriate method for recovering the surface shape. Relaxation method is a suitable method for this purpose.

When the surface is represented as $H = f(x, y)$, the surface normal can be represented by $\mathbf{n} = (p, q, 1)$, where $p = -\partial H/\partial x$ and $q = -\partial H/\partial y$.

To recover the surface shape from surface normal, we calculate the following formula for sufficient times.

$$\begin{aligned} H^{n+1}(x, y) &= \frac{1}{4} \left\{ H^n(x+1, y) + H^n(x-1, y) + H^n(x, y+1) + H^n(x, y-1) \right\} \\ &+ \frac{1}{4} \left\{ \frac{\partial p}{\partial x}(x, y) + \frac{\partial q}{\partial y}(x, y) \right\} . \end{aligned}$$

This method requires a kind of boundary points where the height is already known. We set the boundary of the object as height zero.

Appendix E

English-Japanese Dictionary for Technical Terms

absorptance 吸収率
ambiguity 曖昧性
amplitude 振幅
angular frequency 角周波数
azimuth angle 方位角
blackbody 黒体
body reflection 内部反射
Brewster angle ブリュースタ角
Brewster curve (coined word) ブリュースタ線 (造語)
Brewster point (coined word) ブリュースタ点 (造語)
Brewster segmentation (coined word) ブリュースタ分割 (造語)
charge density 電荷密度
dot product 内積
electric current density 電流密度
electric displacement 電束密度
electric field 電場
electric vector 電気ベクトル
electrolytic polarization 分極
electromagnetic 電磁の
electromagnetic wave 電磁波
elevation angle 仰角
elliptic 楕円の

emissivity 透過率
dielectric 誘電体
dielectric permittivity 誘電率
differential geometry 微分幾何学
folding point (coined word) 折り返し点 (造語)
folding curve (coined word) 折り返し線 (造語)
frequency 周波数
Gaussian curvature ガウス曲率
Gaussian mapping ガウス写像
Gaussian sphere ガウス球
great circle 大円
hyperbolic 双曲の
imaginary number 虚数
incident 入射の
infrared light 赤外光
insulator 絶縁体
intensity 強度
interface 界面, 境界面
isotropic 等方性の
least square method 最小二乗法
magnetic field 磁場
magnetic induction 磁気誘導
magnetic permeability 透磁率
magnetic vector 磁気ベクトル
magnetization 磁化
mean curvature 平均曲率
medium 媒質
normal section 法截面
optics 光学
orientation of the plane of incidence 入射面角度
orthogonal 直交の
parallel 平行の
perpendicular 垂直の
plane of incidence 入射面
plane wave 平面波
polarization 偏光

polarization degree (degree of polarization) 偏光度
position vector 位置ベクトル
principal curvatures 主曲率
principal directions 主方向
principal planes 主平面
propagation vector 伝播ベクトル
reflected 反射の
reflectivity 反射率
refractive index 屈折率
relaxation method 弛緩法
substitute 代入する
surface normal 表面法線
surface reflection 表面反射
thermal equilibrium 熱平衡
thermal radiation 熱放射
thermodynamics 熱力学
toric トーラスの
transmitted 透過の
transmissivity 透過率
transparent object 透明物体
transversal wave 横波
umbilic 臍点
vacuum 真空
visible light 可視光
wavelength 波長
wave vector 波数ベクトル

Appendix F

References Written in Japanese

F.1 References for Computer Visions

1. 岡崎 彰夫, “はじめての画像処理技術,” 工業調査会, 2000.
2. 谷口慶治, “画像処理工学 基礎編,” 共立出版, 1996.
3. 徐 剛, “写真から作る3次元CG イメージ・ベースド・モデリング&レンダリング,” 近代科学社, 2001.
4. 徐 剛, 辻 三郎, “3次元ビジョン,” 共立出版, 1998.
5. 松山隆司, 久野義徳, 井宮 淳 編, “コンピュータビジョン 技術評論と将来展望,” 新技術コミュニケーションズ, 1998.

F.2 References for Optics

1. 左巻健男, 桑嶋 幹, 川口幸人, “光と色の100不思議,” 東京書籍, 2001.
2. 村田和美, “光学,” サイエンス社, 1979.
3. 谷田貝豊彦, “応用光学 光計測入門,” 丸善, 1988.
4. 都筑卓司, “なっとくする音・光・電波,” 講談社, 1998.
5. 大頭 仁, 高木康博, 映像情報メディア学会 編, “基礎光学 一光の古典論から量子論まで,” コロナ社, 2000.

6. 左貝潤一, “光学の基礎,” コロナ社, 1997.
7. 辻内順平, “光学概論 I,” 朝倉書店, 1976.
8. マックス・ボルン, エミル・ウオルフ, “光学の原理 I,” 東海大学出版会, 1974.
9. 會田軍太夫, “光学・光通信のための 波動光学入門,” 東京電機大学出版局, 1980.
10. W. A. シャークリフ, “偏光とその応用,” 共立出版, 1965.
11. 田幸敏治, 辻内順平, 南茂夫, “光測定ハンドブック,” 朝倉書店, 1994.
12. 藤原久利, “LCD 用ガラス基板平坦度計測法,” 三次元工学研究会資料集, 8, 67, (1997).
13. 久保田広, 浮田祐吉, 會田軍太夫, “光学技術ハンドブック,” 朝倉書店, 1976.
14. 土井康弘, “偏光と結晶光学,” 共立出版, 1975.
15. 大津元一, “現代光科学,” 朝倉書店, 1994.
16. 齊藤めぐみ, 佐藤洋一, 池内克史, “ハイライトの偏光解析にもとづく透明物体表面形状の計測,” 情報処理学会コンピュータビジョンとイメージメディア研究会, 98-CVIM-110, March, 1998.
17. 齊藤めぐみ, 佐藤洋一, 池内克史, 柏木 寛, “ハイライトの偏光解析にもとづく透明物体の表面形状測定,” 情報処理学会 画像の認識・理解シンポジウム '98, pp. 53-58, vol.2, July 1998.
18. 齊藤めぐみ, 佐藤洋一, 池内克史, 柏木 寛, “ハイライトの偏光解析にもとづく透明物体の表面形状測定,” 電子情報通信学会論文誌 D-II, Vol. J82-D-II, No. 9, pp. 1383-1390, September 1999.
19. 西野 恒, 原 健二, 高橋 徹, 宮崎大輔, Robby T. Tan, 池内克史, “画像にもとづく見えの解析 —文化財のデジタル化に向けて—,” 計測自動学会第2回システムインテグレーション部門学術講演会 (SI2001), pp.221-222, 2001.12

F.3 References for Thermodynamics

1. 山田克哉, “光と電気のからくり 物を熱するとなぜ光るのか?,” 講談社, 1999.
2. 戸田盛和, “いまさら熱力学?,” 丸善, 1997.

3. イリヤ・プリゴジン, ディリブ・コンデプディ, “現代熱力学 — 熱機関から散逸構造へ,” 朝倉書店, 2001.
4. 藤岡和夫, 小原寛, 齋藤英明, “光・量子エレクトロニクス,” コロナ社, 1991.
5. 赤外線研究会編, “赤外線光学 — 基礎と応用 —,” オーム社, 1991.
6. 斉藤めぐみ, 佐藤洋一, 池内克史, “赤外光の偏光解析とその透明物体形状モデリングへの応用,” (Polarization Analysis of Infrared Emission for Shape Measurement of Transparent Objects) 画像の認識・理解シンポジウム (MIRU2000), 講演論文集 I, pp.95-100, 7月, 2000.
7. 斉藤めぐみ, 佐藤洋一, 池内克史, “赤外線の偏光解析とその透明物体形状モデリングへの応用,” 情報処理学会論文誌: コンピュータビジョンとイメージメディア「Physics-based VisionとCGの接点」特集号, Vol.41・SIG10, pp.12-18, December, 2000.

F.4 References for Differential Geometries

1. 川久保勝夫, “トポロジーの発想 \circ と \triangle を同じと見ると何が見えるか,” 講談社, 1995.
2. 上野健爾, 志賀浩二, 森田茂之, “高校生に贈る数学 I,” 岩波書店, 1995.
3. 志賀浩二, “数学が育っていく物語 第6週 曲面,” 岩波書店, 1994.
4. 小林昭七, “曲線と曲面の微分幾何,” 裳華房, 1977.
5. 長野 正, “曲面の数学,” 培風館, 1968.
6. 佐々木重夫, “岩波講座 基礎数学 幾何学 V 微分幾何学 I — 曲面論 —,” 岩波書店, 1977.
7. 佐々木重夫, “岩波講座 基礎数学 幾何学 V 微分幾何学 II — 曲面論 —,” 岩波書店, 1977.